

Article

# Impacts of Clear-Cutting of a Boreal Forest on Carbon Dioxide, Methane and Nitrous Oxide Fluxes

Patrik Vestin <sup>1,\*</sup>, Meelis Mölder <sup>1</sup>, Natascha Kljun <sup>2</sup>, Zhanzhang Cai <sup>1</sup>,  
Abdulghani Hasan <sup>1</sup>, Jutta Holst <sup>1</sup>, Leif Klemedtsson <sup>3</sup> and Anders Lindroth <sup>1</sup>

<sup>1</sup> Department of Physical Geography and Ecosystem Science, Lund University, Sölvegatan 12, 223 62 Lund, Sweden; meelis.molder@nateko.lu.se (M.M.); zhanzhang.cai@nateko.lu.se (Z.C.); abdulghani.hasan@nateko.lu.se (A.H.); jutta.holst@nateko.lu.se (J.H.); anders.lindroth@nateko.lu.se (A.L.)

<sup>2</sup> Centre for Environmental and Climate Research, Lund University, Sölvegatan 37, 223 62 Lund, Sweden; natascha.kljun@cec.lu.se

<sup>3</sup> Department of Earth Sciences, University of Gothenburg, Guldhedsgatan 5A, 405 30 Gothenburg, Sweden; leif.klemedtsson@gvc.gu.se

\* Correspondence: patrik.vestin@nateko.lu.se

Received: 7 August 2020; Accepted: 27 August 2020; Published: 1 September 2020



**Abstract:** The 2015 Paris Agreement encourages stakeholders to implement sustainable forest management policies to mitigate anthropogenic emissions of greenhouse gases (GHG). The net effects of forest management on the climate and the environment are, however, still not completely understood, partially as a result of a lack of long-term measurements of GHG fluxes in managed forests. During the period 2010–2013, we simultaneously measured carbon dioxide (CO<sub>2</sub>), methane (CH<sub>4</sub>) and nitrous oxide (N<sub>2</sub>O) fluxes using the flux-gradient technique at two clear-cut plots of different degrees of wetness, located in central Sweden. The measurements started approx. one year after clear-cutting, directly following soil scarification and planting. The study focused on robust inter-plot comparisons, spatial and temporal dynamics of GHG fluxes, and the determination of the global warming potential of a clear-cut boreal forest. The clear-cutting resulted in significant emissions of GHGs at both the wet and the dry plot. The degree of wetness determined, directly or indirectly, the relative contribution of each GHG to the total budgets. Faster establishment of vegetation on the wet plot reduced total emissions of CO<sub>2</sub> as compared to the dry plot but this was partially offset by higher CH<sub>4</sub> emissions. Waterlogging following clear-cutting likely caused both plots to switch from sinks to sources of CH<sub>4</sub>. In addition, there were periods with N<sub>2</sub>O uptake at the wet plot, although both plots were net sources of N<sub>2</sub>O on an annual basis. We observed clear diel patterns in CO<sub>2</sub>, CH<sub>4</sub> and N<sub>2</sub>O fluxes during the growing season at both plots, with the exception of CH<sub>4</sub> at the dry plot. The total three-year carbon budgets were 4107 gCO<sub>2</sub>-equivalent m<sup>-2</sup> and 5274 gCO<sub>2</sub>-equivalent m<sup>-2</sup> at the wet and the dry plots, respectively. CO<sub>2</sub> contributed 91.8% to the total carbon budget at the wet plot and 98.2% at the dry plot. For the only full year with N<sub>2</sub>O measurements, the total GHG budgets were 1069.9 gCO<sub>2</sub>-equivalents m<sup>-2</sup> and 1695.7 gCO<sub>2</sub>-equivalents m<sup>-2</sup> at the wet and dry plot, respectively. At the wet plot, CH<sub>4</sub> contributed 3.7%, while N<sub>2</sub>O contributed 7.3%. At the dry plot, CH<sub>4</sub> and N<sub>2</sub>O contributed 1.5% and 7.6%, respectively. Our results emphasize the importance of considering the effects of the three GHGs on the climate for any forest management policy aiming at enhancing the mitigation potential of forests.

**Keywords:** CO<sub>2</sub>; CH<sub>4</sub>; N<sub>2</sub>O; greenhouse gas budget; clear-cutting; boreal forest; forest management

## 1. Introduction

Forests play an important role in the mitigation of fossil fuel emissions by sequestering atmospheric carbon dioxide. Pan, Birdsey [1] estimated the global annual forest sink to be  $2.4 \pm 0.4$  Pg C on average

(1990–2007). Forests, thus, constitute by far the largest share of the terrestrial carbon sink [2]. This sink abates about 25% of the global fossil fuel emissions ( $10.0 \pm 0.5 \text{ Pg C year}^{-1}$  in 2018 [3]) which is a considerable contribution towards mitigation of anthropogenic emissions. Other studies have suggested even larger mitigation potential of forests through management [4]. The forest sector is also pointed out in Article 5 of the 2015 Paris Agreement as one of the key components of the mitigation work [5]. However, the management of forests can impact the environment in many different ways as it affects both greenhouse gas (GHG) exchanges and energy exchange. Luysaert, Marie [6] argued that additional climate benefits from forest management would be small and local rather than global and Naudts, Chen [7] showed that two and a half centuries of forest management in Europe had not reduced climate warming, in spite of considerable afforestation efforts. In fact, the net outcome was a slight warming effect. This clearly demonstrates that forest management for mitigation purposes requires expert knowledge of its complex impacts on the climate system.

Even-aged forestry is the dominating silvicultural method in Sweden and in most of the boreal region. A typical rotation cycle consists of clear-cutting, soil scarification, plantation and one to three forest thinnings before it is time for clear-cutting again. Clear-cutting and the subsequent soil preparation cause major disturbance of the ecosystem. In Sweden, an average of 195 600 ha was clear-cut annually during the period 2004–2013 [8]. An average of ~88% of this area also underwent soil scarification and ~83% of the area was subsequently planted.

The removal of trees through clear-cutting can have many consequences for the climate and the environment. Reduced photosynthesis, reduced autotrophic respiration and increased heterotrophic respiration following harvest affect the  $\text{CO}_2$  budget, but the extent and the net result depend on ecosystem type, climate, soil conditions, the severity of the soil disturbance, etc., and on how long time it takes for the vegetation cover to be re-established. Clear-cutting also affects the biophysical feedback mainly through albedo changes [7].

In addition, fluxes of other greenhouse gases such as methane ( $\text{CH}_4$ ) and nitrous oxide ( $\text{N}_2\text{O}$ ) can also be significant in forest ecosystems but there is a lack of knowledge of how these fluxes are affected by forest management. Generally, forest soils are net sinks of  $\text{CH}_4$  [9]. Methane is consumed by methanotrophic bacteria in aerobic parts of soils [10] while  $\text{CH}_4$  production by archaea may take place in the water-saturated parts of soils [11], and at anaerobic micro-sites in soils [12]. Reduced evapotranspiration after harvest can result in a raised water table and reduced methane ( $\text{CH}_4$ ) uptake, or even cause a switch from a sink to a source of  $\text{CH}_4$  [13–16]. However, methane consumption in soils is an important net sink of atmospheric methane, second only to tropospheric oxidation by OH radicals. The global sink strength was recently estimated to be 28–32 Tg  $\text{CH}_4 \text{ year}^{-1}$  [17]. Several studies [18,19] have shown that the sink strength of forest soils is larger than for other land cover classes, indicating that the global methane budget is sensitive to disturbances of forests. Yu, Huang [19] recently estimated the global forest soil sink strength to be 9.16 ( $\pm 3.84$ ) Tg  $\text{CH}_4 \text{ year}^{-1}$  during the period 1981–2010. Ni and Groffman [20] reported a 77% decrease in forest soil  $\text{CH}_4$  uptake during 1988–2015 at measurement sites around the world. The decrease was especially pronounced in forests located between  $0^\circ$  and  $60^\circ \text{ N}$  where precipitation had increased during the same time period.

Nitrous oxide production is dependent on mineralization and immobilization rates in soils, which control substrate availability for soil microbes.  $\text{N}_2\text{O}$  production takes place mainly through microbe-mediated processes (i.e., nitrification, denitrification, nitrate ammonification and nitrifier denitrification), with nitrification and denitrification contributing approx. 70% to the total global emissions from soils [21].  $\text{N}_2\text{O}$  produced in soils can be reduced to  $\text{N}_2$  through denitrification [22] and nitrifier denitrification ([23]) and result in reduced net emissions, or in some cases even in a net uptake of atmospheric  $\text{N}_2\text{O}$  [24–28]. Chapuis-Lardy, Wrage [29] reviewed the available literature and attributed net  $\text{N}_2\text{O}$  uptake to denitrification, often in connection with low mineral nitrogen content and low oxygen availability in the soils. Production, as well as consumption of  $\text{N}_2\text{O}$ , is regulated at different scales (from microsites to landscape level) by a large number of variables that are interconnected in a complex manner [30]. This results in large spatial and temporal variability in  $\text{N}_2\text{O}$  fluxes and is further

complicated by the fact that low fluxes of  $N_2O$  may result from a large number of processes other than nitrification and denitrification [21]. It is thus important to measure  $N_2O$  fluxes with techniques that are both spatially and temporally integrating, in order to generate accurate annual estimates of fluxes [31].

Eddy covariance (EC) studies on forest chronosequences have shown that clear-cuts remain carbon sources for 10–18 years after harvest [32–34]. Coursolle, Margolis [34] studied six Canadian chronosequences (two burned, three harvested and one afforestation) and found that it took an average of 26 years to compensate for the initial carbon losses in harvested Canadian boreal forests. Lindroth, Lagergren [35] generalized the results from four European chronosequence studies [36–39] and found a relationship between net ecosystem productivity and relative stand age (defined as normal stand age divided by the typical rotation length for each forest chronosequence), indicating that clear-cut sites were carbon sources for about 15% of the relative age, which corresponds to approx. 9–18 years for typical Swedish rotation lengths. Apart from the above-mentioned chronosequence studies, relatively few EC  $CO_2$  studies have been made at clear-cut sites [15,40–47].

Relatively few micrometeorological studies of  $CH_4$  or  $N_2O$  fluxes have been made in forest ecosystems in general [24–26,48–53]. Zona, Janssens [54] measured  $CO_2$ ,  $CH_4$  and  $N_2O$  fluxes above a short-rotation poplar plantation in Belgium, Gao, Chen [55] performed EC measurements of  $CO_2$  and  $CH_4$  in a poplar plantation in subtropical China and Mishurov and Kiely [56] did EC measurements of  $N_2O$  fluxes on afforested grassland. We are not aware of any studies using simultaneous micrometeorological measurements of  $CO_2$ ,  $CH_4$  and  $N_2O$  at a clear-cut boreal forest stand.

The chamber technique, on the other hand, has been widely used for measurements of fluxes of  $CO_2$  [41,57–60],  $CH_4$  [14,61,62],  $N_2O$  [63,64] or combinations of different greenhouse gases [15,16,27,28,32,65–68] on clear-cuts. Although chamber measurements can provide useful information on GHG fluxes from well-defined source areas with known conditions (soil temperature, soil moisture, pH, C:N ratio, etc.), the poor spatial—often along with a poor temporal—representation of these measurements make it difficult to study GHG dynamics and to derive reliable estimates of full long-term GHG budgets [21].

Thus, a knowledge gap exists and there is an obvious need for long-term, continuous GHG measurements that integrate over larger areas on clear-cuts. As pointed out by Oren, Hsieh [69], usually only one EC tower is used to represent ecosystem fluxes although the spatial variability within an ecosystem can be large. Hill, Chocholek [70] recently highlighted the importance of spatial replication of EC measurements to derive statistically robust flux estimates for a given ecosystem. However, long-term simultaneous multi-tower EC measurements of  $CO_2$ ,  $CH_4$  and  $N_2O$  are expensive, technically challenging and require frequent calibrations and maintenance of the equipment in order to make accurate and comparable measurements. An alternative approach to EC measurements is to do flux-gradient measurements [53,71] using only one set of gas analyzers in a multi-tower setup. This approach has the benefit of making comparisons of fluxes between plots more robust since the same instruments analyze gases from all plots, at the same time as the total cost and need for maintenance and calibrations are greatly reduced.

The main objectives of this study were (i) to develop a system for continuous multi-plot measurements of fluxes of  $CO_2$ ,  $CH_4$  and  $N_2O$  that minimizes cost and need for maintenance and at the same time makes inter-plot comparisons more robust; (ii) to study the temporal and spatial dynamics of GHG fluxes; and (iii) to quantify GHG exchange and estimate full GHG budgets following clear-cutting.

## 2. Materials and Methods

### 2.1. Site Description

The study site is located in a hemiboreal forest in close vicinity of the ICOS (Integrated Carbon Observation System) Sweden station Norunda (60°5' N, 17°29' E) in central Sweden (Figure 1). Mean air temperature at Uppsala, 30 km south of Norunda, was 6.5 °C while mean annual precipitation was

575.6 mm (1981–2010). The soil is a sandy-loamy glacial till with a high content of stones and blocks [72], covered with a thin organic layer (3–10 cm thick). The pre-harvest forest was a mixed Scots pine (*Pinus sylvestris*, 58%) and Norway spruce (*Picea abies*, 40.5%) stand, with a small fraction of birch (*Betula* sp., 1.5%). Before harvest, the ground vegetation was dominated by bilberry (*Vaccinium myrtillus*) and feather mosses (*Hylocomium splendens* and *Pleurozium schreberi*). The forest stand (~30 ha) was harvested in early 2009 (Figure 1) and was subsequently soil scarified (mounding or harrowing) and replanted in May 2010. Approximately 2500 seedlings ha<sup>-1</sup> were planted (50% each of Scots pine and Norway spruce). Following harvest, grasses and shrubs quickly dominated the site, which, together with changes in hydrology, had a negative impact on the survival rate of the seedlings. Hence, in May 2012, an additional 2200 seedlings ha<sup>-1</sup> (100% Norway spruce) were planted.

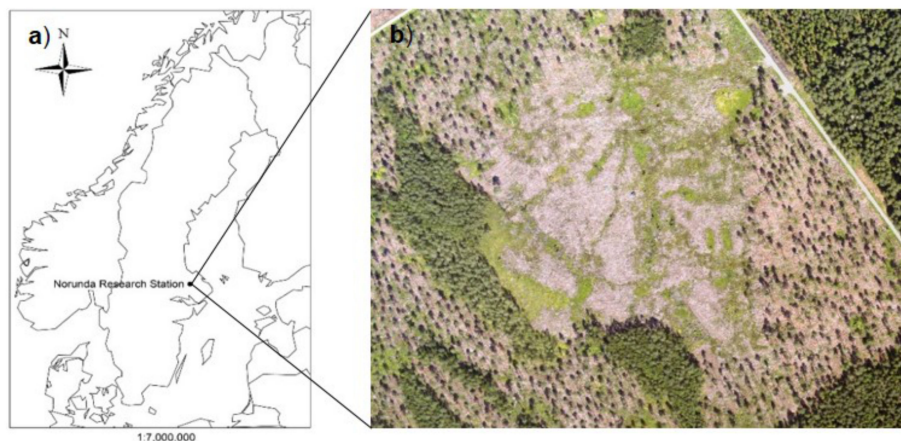


**Figure 1.** Location of the ICOS Sweden station Norunda (60°5' N, 17°29' E) in central Sweden (a) and the clear-cut in the close vicinity of the Norunda station where the study took place (b). The forest was harvested in 2009 and measurements started at the new clear-cut in May 2010 following soil scarification and planting. The aerial photograph was captured in 2011 during an airborne LiDAR campaign.

Four experimental plots with a diameter of approximately 100 m were established on the new clear-cut during the summer of 2009. For this study, only measurements from plots 1 and 2 (Figure 2) were used, as plots 3 and 4 received a different treatment.

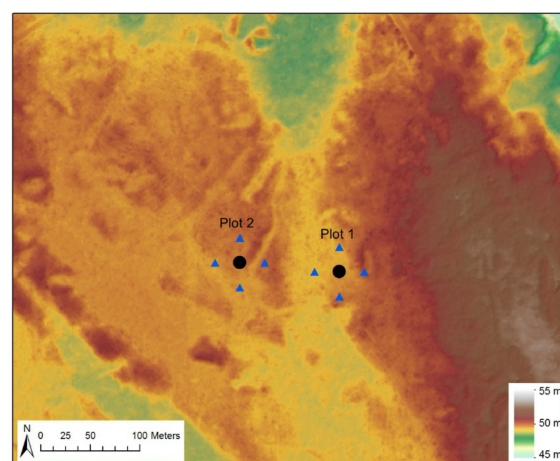


**Figure 2.** Digital Elevation Model (DEM) of the study area. The DEM was generated using data from a high spatial resolution airborne LiDAR survey in 2011 and shows the height above sea level for each square meter of the study area. The black circles depict the tower locations of plot 1 and plot 2. The blue triangles represent groundwater pipes installed down to 2.5 m depth, 25 m North, East, South and West of each tower.

## 2.2. Data Collection and Raw Data Processing

### 2.2.1. Environmental Variables

Directly following soil scarification in May 2010, sensors for measurements of soil temperature and soil moisture were installed at different depths at a location considered to be representative for both plots (at plot 2, bordering plot 1). Soil temperatures were measured at 5, 10, 20, 30 and 40 cm depth with copper-constantan thermocouples. Soil moisture was measured at 5, 20 and 40 cm depth (ML2x ThetaProbe, Delta-T Devices Ltd., Cambridge, UK). Precipitation was measured at 1 m height (rain and snow gauge with a heated funnel and base, Series 375, Met One Instruments, Inc., Grants Pass, OR, USA) at the center of the clear-cut. Four groundwater pipes were installed on each plot to allow for monitoring of groundwater level and for groundwater sampling. The pipes were drilled down to 2.5 m depth, 25 m North, East, South and West of the center of each plot (Figure 2). Groundwater level was continuously measured (Druck PDCR 1830, GE-sensing, Billerica, MA, USA) at one location (L1) on plot 2 (25 m North of the center of the plot) from October 2010 onwards. The groundwater levels in all eight pipes were manually measured multiple times in 2010 and in 2012. From the DEM (Figure 2) the differences in elevation at the ground surface between pipe L1 and the other seven pipes on plots 1 and 2 were calculated. This allowed for generating time series with daily average data on groundwater level for all eight pipes on plots 1 and 2 by assuming that groundwater levels at the other seven pipes were related to water table fluctuations at L1. These data were used to interpolate groundwater surfaces for plots 1 and 2 using kriging [73], and to estimate the distance between the groundwater level and the soil surface for each cell in the DEM (cell size 1 m<sup>2</sup>). Daily average distances between the soil surface and the interpolated groundwater surfaces were calculated. The manual pipe measurements were used for validation of the estimated groundwater levels.

A short mast was installed centrally at the clear-cut site, close to the edge of plot 2, for measurements of net radiation (NR-lite net radiometer, Kipp and Zonen, Delft, The Netherlands) and air temperature. Air temperature was measured with a copper-constantan thermocouple in an aspirated radiation shield at 2 m height. Two web cameras (Mobotix M24M, Mobotix AG, Haupsitz, Germany) mounted on a 25 m tall mast took hourly digital photographs of both plots during daylight conditions (Figure 3), which allowed to track vegetation development and to detect when the ground was snow-covered. In addition, data on global radiation, incoming PAR, air temperature, air pressure, relative humidity and snow depth were further obtained from the Norunda main tower site, 600 m from the center of the clear-cut, either to complement existing measurements or to fill shorter gaps arising from power failures, etc.

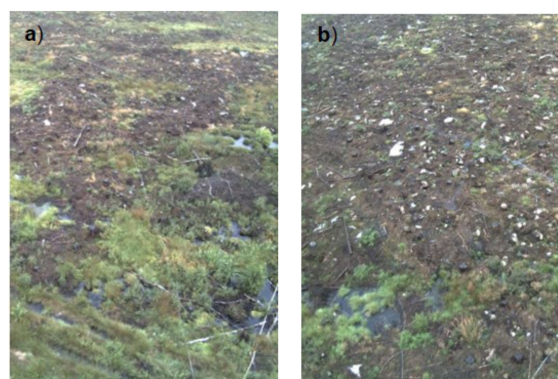


**Figure 3.** Digital camera images of a part of plot 1 (a) and of a part of plot 2 (b) taken on the same day in mid-August 2011. The images cover approx. 40 × 60 m of each plot. Large areas with standing water can be seen in the lower half of the image of plot 1. A small area with standing water can be seen in the lower left part of the image of plot 2, but this plot was in general drier than plot 1. The vegetation cover on both plots was dominated by grasses and shrubs, as most evident on plot 1.

### 2.2.2. Gradient Measurements

A 3 m tall tower was erected at the center of each plot and was equipped for measurements of turbulence parameters and concentrations of CO<sub>2</sub>, H<sub>2</sub>O, and CH<sub>4</sub> (May 2010–May 2013) as detailed below. Because of instrumental problems with the original gas analyzer, N<sub>2</sub>O measurements were only undertaken from June 2011 to September 2012.

Wind and turbulence parameters were measured at 2.5 m height by sonic anemometers (Gill Windmaster, Gill Instruments Ltd., Hampshire, UK) at a frequency of 20 Hz. Data from the sonic anemometers were recorded on a computer. Air was continuously pulled (flow rates > 2.0 l min<sup>-1</sup>) from two heights at each tower through 100 m long high-density polyethylene tubes (inner diameter 8 mm) to a manifold inside a measurement hut placed centrally on the clear-cut. This setup where air was pulled from all intakes simultaneously to the manifold allowed for fast switching between the air intakes. The air intakes had 7 µm filters, were heated and had an orifice to create underpressure and prevent condensation of water vapor in the tubes. The intakes were placed at 0.6 m and 2.0 m height at the start of the measurements but the lower intakes were raised to 0.8 m in June 2012 to adjust for the increased height of the ground vegetation. The air stream from the intakes was analyzed for CH<sub>4</sub>, CO<sub>2</sub> and H<sub>2</sub>O with a Los Gatos tunable diode laser spectrometer (DLT-100, Los Gatos Research, San Jose, CA, USA) and N<sub>2</sub>O and H<sub>2</sub>O (QCL Mini Monitor, Aerodyne Research, Inc., Billerica, MA, USA) at a rate of 1 Hz. The data were recorded by a CR1000 datalogger (Campbell Scientific, Logan, UT, USA). Each location was sampled for 15 min each hour. These 15 mins were set up such that each level was sampled for 150 s before switching to the next level. The first 45 s of data from each level were discarded while the remaining data was used to calculate an average concentration for the two levels (N = 315 per level) during the 15-min period. Hence, an average concentration gradient for each of the gas species could be calculated once per hour and tower. These gradients were assumed to be representative for the full hour. Gas concentration data were quality controlled and filtered based on absolute limits wide enough to allow for high concentration values during stable stratification (300–800 ppm for CO<sub>2</sub>, 1.5–4.0 ppm for CH<sub>4</sub>, 0–30,000 ppm for H<sub>2</sub>O and 300–600 ppb for N<sub>2</sub>O). Gas concentration data were also filtered based on standard deviation following Schmid, Grimmond [74]:

$$|C_i - \bar{C}_j| \geq D \cdot \sigma_j \quad (1)$$

Any concentration value  $C_i$  that deviated more than the product of a discrimination factor  $D$  and the standard deviation  $\sigma_j$  from the mean concentration  $\bar{C}_j$  over the averaging interval was considered a spike and was removed. This was an iterative process where  $D$  increased from 3.5 to 5.0 in steps of 0.3.

Gas concentrations were corrected for dilution effects by water vapor. In addition, CH<sub>4</sub> and N<sub>2</sub>O concentrations were also corrected for dilution by CO<sub>2</sub>. All concentrations were converted from µmol mol<sup>-1</sup> to µmol m<sup>-3</sup> using the ideal gas law and measurements of air temperature and air pressure. A linear decrease in air pressure of 12.5 Pa m<sup>-1</sup> with height was assumed in the conversions at the two measurement heights.

### 2.2.3. Eddy Covariance Data

The sensible heat fluxes, friction velocities and Obukhov lengths (all derived from the sonic anemometer measurements) needed for estimating gas fluxes were calculated with the EddyPro software, version 5.0 (LI-COR, Lincoln, NE, USA), following standard eddy covariance methods. Turbulent fluctuations of the times series data were extracted using block-averaging over 15-min intervals corresponding to the gradient measurements. Raw data were de-spiked following Vickers and Mahrt [75] before calculating fluxes. Data failing statistical tests for spike count, absolute limits, discontinuities and angle of attack were discarded from further analysis. The following corrections were applied; cross-wind correction for sonic temperature (applied directly by the anemometer firmware), angle of attack [76], double rotation for tilt correction, high-pass filtering [77] and low-pass filtering [78]. Ogive tests [79,80] showed that 15-min averaging intervals were sufficient to capture most of the low-frequency contributions to the fluxes under turbulent conditions.

#### 2.2.4. Flux-Gradient Calculations

Greenhouse gas exchanges between the ecosystem and the atmosphere were determined using an integrated eddy covariance and gradient method (flux-gradient (FG)). The method is based on Monin–Obukhov similarity theory and is described in detail by Simpson, Edwards [53] and Denmead [71]. Vertical turbulent fluxes  $F_x$  of trace gases can be estimated as the product of the vertical concentration gradient of the gas species  $x$  times its turbulent diffusivity:

$$F_x = -K_x \frac{\partial C_x}{\partial z} \quad (2)$$

where  $K_x$  is the turbulent diffusivity ( $\text{m}^2 \text{s}^{-1}$ ) of gas  $x$ ,  $C_x$  is the concentration ( $\mu\text{mol m}^{-3}$ ) of gas  $x$  and  $z$  (m) is the measurement height. To account for non-neutral atmospheric conditions,  $K_x$  can be expressed as

$$K_x = \frac{\kappa u_* z}{\varphi_H(\zeta)} \quad (3)$$

where  $\kappa$  is the von Kármán constant (0.40, following Högström [81]),  $u_*$  is the friction velocity,  $\varphi_H$  is the universal function for sensible heat and  $\zeta$  is a dimensionless stability parameter. The universal function for sensible heat is commonly used for trace gases and latent heat [82] (p. 58). The stability parameter  $\zeta$  can be expressed as [82] (p. 55):

$$\zeta = \frac{z}{L} = -\frac{\kappa \frac{g}{\theta_s} \frac{H}{\rho C_p} z}{u_*^3} \quad (4)$$

where  $L$  is the Obukhov length,  $g$  is the gravity ( $9.81 \text{ m s}^{-2}$ ),  $\theta_s$  is the characteristic potential temperature,  $\rho$  is the air density,  $C_p$  is the specific heat capacity of air at constant pressure and  $H$  is the sensible heat flux.

Equations (2) and (3) have to be integrated for an atmospheric layer between the air sampling heights  $z_1$  (lower) and  $z_2$  (upper), and adjusted for the zero-displacement height  $d$ . With that,  $F_x$  can be expressed as

$$F_x = -\frac{\kappa u_* (C_{x,z_2} - C_{x,z_1})}{\ln\left(\frac{z_2-d}{z_1-d}\right) - \Psi(\zeta)_{z_2} + \Psi(\zeta)_{z_1}} \quad (5)$$

where  $\Psi(\zeta)$  is the integrated form of the universal function [81].

The zero-displacement height  $d$  and roughness length  $z_o$  were estimated from wind profile measurements during the summer of 2012. Five cup anemometers (cup array from ARI-49 (former USSR), mechanics and electronics developed by Tartu Observatory, Tartu, Estonia) were installed between 1 and 4 m height at a small mast placed centrally at the clear-cut. The cup anemometers were calibrated before and after the measurement period to make sure the obtained wind profiles were of high quality. The estimated  $d$  (0.2 m) and  $z_o$  (0.07 m) were assumed to be valid for both plots throughout the measurement period (2010–2013) but were adjusted depending on the presence of snow ( $z_o$ ) and on the thickness of the snow cover ( $d$ ). The roughness length for a flat snow cover can be in the order of 0.001 m [83], but due to the small variations in topography, tree stumps, etc., at our plots, we chose a slightly higher value (0.003 m) for thick snow covers and an intermittent value between the two cases when the snow cover was thinner than the estimated  $d$ . The choice of  $d$  and  $z_o$  does not affect the calculation of flux values but has an effect on footprint calculations (mostly  $z_o$ ). See Table 1 for details.

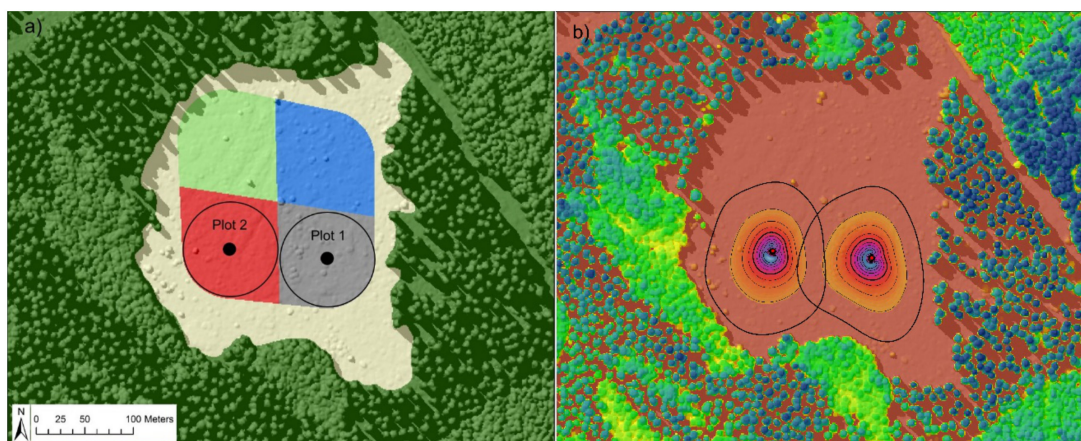
#### 2.3. Footprint Modeling

Figure 4a shows a land cover classification map of the clear-cut site, derived from a field survey of the plot treatment and from an airborne LiDAR survey in 2011. The two-dimensional footprint parametrization of Kljun, Calanca [84] was used for calculating hourly flux footprints for plots 1

and 2. From the footprint climatologies, derived by accumulating these hourly footprints for the whole measurement period, it can already be seen that the fluxes measured at each plot can be contributed to the corresponding land cover class to the largest part (up to 80%, see Figure 4b). Finally, merging hourly footprints with the land cover map allowed for estimating flux contributions per unit area (% per  $\text{m}^2$ ) from the six land cover classes (class 1–4: plots 1–4; class 5: clear-cut and soil scarified area surrounding all plots; class 6: harvested and soil scarified area where widely spaced seed trees were left until 2012). See Figure 4 for details. Following Horst [85], the flux footprint modeling is based on the assumption that the flux footprint is representative for flux-gradient footprints obtained when the measurement height is defined as the arithmetic mean height of the two concentration measurements for stable stratification and is defined as the geometric mean height for unstable stratification.

**Table 1.** Values of displacement height  $d$  and roughness length  $z_0$  used throughout the measurement period (2010–2013), depending on snow cover thickness. The values for snow-free conditions were determined experimentally in situ, while roughness lengths for different snow conditions were estimated based on available literature and site characteristics.

Snow Depth (m)	Displacement Height $d$ (m)	Roughness Length $z_0$ (m)
0	0.2	0.07
$0 \geq 0.2$	0.2	0.03
$>0.2$	Actual snow depth	0.003



**Figure 4.** (a) Schematic picture of the land cover classifications: grey, red, blue and green fields represent footprint classes 1–4 (plots 1–4, only plots 1 and 2 are included in this study), respectively; yellow represents class 5 and dark green represents class 6. The black circles represent the maximum hourly footprint extent (50 m radius) allowed in the strictest filtering of the flux data (see Section 2.4 for details). (b) Footprint climatology, i.e., hourly flux footprints cumulated for the whole year 2012. Each of the black contour lines represents 10% contribution to the aggregated flux footprint, up to a maximum of 90%. The red circles represent the tower locations. The outermost contour line represents 90% contribution to the aggregated footprints. Due to significant overlap of these footprints, only contributions up to 80% were considered. The background map depicts the tree cover derived from a LiDAR survey in 2011.

#### 2.4. Flux Data Filtering

Data quality tests on developed turbulent conditions and steady-state conditions were performed according to Mauder and Foken [86], resulting in a quality flag system (0–1–2) of the data. Sensible heat flux data with flag 2 were discarded from further analyses.

The errors of the gradient measurements were estimated to be  $0.3 \text{ nmol mol}^{-1}$  ( $\text{CH}_4$ ),  $0.15 \text{ } \mu\text{mol mol}^{-1}$  ( $\text{CO}_2$ ) and  $4000 \text{ } \mu\text{mol mol}^{-1}$  ( $\text{H}_2\text{O}$ ) for LGR data and  $0.028 \text{ nmol mol}^{-1}$  ( $\text{N}_2\text{O}$ ) and  $1400 \text{ } \mu\text{mol mol}^{-1}$  ( $\text{H}_2\text{O}$ ) for Aerodyne data, based on lab tests of the instruments RMS noise. Maximum errors in turbulent

diffusivities were found to be  $0.02 \text{ m s}^{-1}$  for all conditions with  $u_* > 0.06 \text{ m s}^{-1}$  and hence, data collected during periods of  $u_* < 0.06 \text{ m s}^{-1}$  were discarded from further analyses. Total errors of the GHG fluxes were estimated as the quadratic sums of errors in fluxes caused by the gradient estimations and by errors in fluxes caused by estimations of the turbulent diffusivities. Data were discarded when the total error of the GHG fluxes was larger than  $2 \mu\text{mol m}^{-2} \text{ s}^{-1}$  ( $\text{CO}_2$ ),  $20 \mu\text{mol m}^{-2} \text{ h}^{-1}$  ( $\text{CH}_4$ ) or  $40 \mu\text{g m}^{-2} \text{ h}^{-1}$  ( $\text{N}_2\text{O}$ ).

Careful examination of the flux data revealed a friction velocity dependency of the fluxes. The threshold where fluxes no longer increased with increasing  $u_*$  varied slightly between seasons and between years but average  $u_*$  thresholds of  $0.16 \text{ ms}^{-1}$  (plot 1) and  $0.15 \text{ ms}^{-1}$  (plot 2) were used for filtering out low-quality data during 2010–2013.

The GHG flux data were further filtered according to the flux footprints in two different ways. Firstly, hourly flux data were filtered according to the 80% footprint extent, ensuring a relatively homogeneous source area; i.e., fluxes with an 80% footprint extending outside the 50 m radius (black circles in Figure 4a) were discarded from further analysis. This approach minimized any possible contributions to the measured fluxes from other land-cover classes and allowed for a more direct comparison of the net GHG fluxes at plots 1 and 2, at the cost of total data coverage. This filtering approach is in the following referred to as footprint extent. Secondly, flux data were filtered according to the footprint classification, which, since it was based on the real plot geometry, maximized the plot areas (see Figure 4a for details). Small contributions (<10%) to the measured fluxes that originated from other land cover classes were allowed. This approach minimized data loss and these data were then gap-filled to derive GHG budgets. This filtering approach is in the following referred to as footprint classification. Despite the very strict filtering on footprint extent (and on all other criteria mentioned above), 21.3–30.6% of data (all GHGs, both plots) still remained for direct inter-plot comparisons. The data filtering on footprint classification resulted in 37.3–57.3% of data remaining for creating GHG budgets on both plots.

By selecting data (filtered for footprint extent) measured during the same hour on both plots, possible problems with temporal autocorrelation of the fluxes were reduced and a non-parametric paired statistical test was carried out (Wilcoxon signed-rank test for zero median) in Matlab.

All gradients, turbulent diffusivities, statistics and final GHG fluxes were calculated with Matlab R2015b (Mathworks, Inc., Natick, MA, USA).

## 2.5. Gap-Filling, Flux-Partitioning and Global Warming Potential

### 2.5.1. $\text{CO}_2$ Flux Data

Gaps in  $\text{CO}_2$  flux data were filled using the R software (version 3.3.2) and the R package *REddyProc* [87]. *REddyProc* is a gap-filling and flux-partitioning tool that follows Reichstein, Falge [88]. In short, gaps in data are filled with average values during similar meteorological conditions (or during the same time of the day in case no meteorological data were available) for a time window of varying size.

Only original data passing quality tests and filtering were used for flux-partitioning. The flux-partitioning assumes zero gross primary productivity (*GPP*) during night-time, i.e., the measured net ecosystem exchange (*NEE*) equals total ecosystem respiration ( $R_{eco}$ ) when global radiation  $< 20 \text{ Wm}^{-2}$ . The Lloyd and Taylor [89] model is then used to derive an empirical model of  $R_{eco}$  based on air temperature ( $T$ ):

$$R_{eco} = R_{eco,T_{ref}} \cdot e^{E_0 \left( \frac{1}{T_{ref}-T_0} - \frac{1}{T-T_0} \right)} \quad (6)$$

where  $R_{eco,T_{ref}}$  is base respiration at reference temperature  $T_{ref}$  (set to  $10 \text{ }^\circ\text{C}$ ),  $E_0$  ( $^\circ\text{C}$ ) is the temperature sensitivity,  $T_0$  is kept constant at  $-46.02 \text{ }^\circ\text{C}$  as in Lloyd and Taylor [89].  $E_0$  and  $R_{eco,T_{ref}}$  are then estimated for each flux-averaging interval, resulting in hourly estimates of  $R_{eco}$ . Ecosystem respiration was extrapolated to daytime conditions using daytime air temperature. *GPP* was estimated as the difference

between measured  $NEE$  and modeled  $R_{eco}$ . See Reichstein, Falge [88] and Wutzler, Lucas-Moffat [87] for a more detailed description of the gap-filling and flux-partitioning procedures.

### 2.5.2. CH<sub>4</sub> and N<sub>2</sub>O Flux Data

It was not possible to find strong relationships between methane exchange and different environmental variables at the clear-cut plots. Hence, data gaps were filled using linear interpolation of daily average methane fluxes. Daily average methane fluxes were calculated for days with at least six hourly measurements passing all filtering criteria and with outliers ( $\sigma > 5$ ) removed prior to the averaging.

Gaps in N<sub>2</sub>O flux data were filled using linear interpolation of daily averaged data, similar to the method used by Scanlon and Kiely [90]. Daily averages were calculated in the same way as for the CH<sub>4</sub> data.

### 2.5.3. Global Warming Potential

For direct comparisons of the relative importance of the different GHGs, gap-filled CH<sub>4</sub> and N<sub>2</sub>O fluxes were also converted into CO<sub>2</sub>-equivalents by multiplication with a global warming potential factor in a 100-year perspective (GWP<sub>100</sub>) of 28 (CH<sub>4</sub>) and 265 (N<sub>2</sub>O) [91].

## 2.6. Vegetation Development

Landsat images with a spatial resolution of 30 m × 30 m were used to estimate vegetation cover on each of the experimental plots during the main growing seasons (June, July and August) of 2005 to 2014. The study site was captured by three stacks (paths 192–194; row 18) from Landsat 4, 5, and 7. Overlap among these three stacks was used to build up a high-resolution vegetation index time series for each of the experimental plots. High-quality data were identified by Fmask, which was used for automated detection of clouds, cloud shadows and snow masking for Landsat TM/ETM+ images [92,93]. The growing season Normalized Difference Vegetation Index (NDVI) [94] of each plot was calculated by averaging all high-quality Landsat data for 3 × 3 pixels during summer (JJA) of each year of the study period. These 90 m × 90 m areas overlapped the areas specified by the footprint classification (Figure 4a) by 70–85%.

## 3. Results

### 3.1. Environmental Conditions

The mean air temperature for the three study years (with a year defined as May 20 to May 19 of the following year in order to match the flux measurement periods) was 5.0 °C, 6.9 °C and 4.9 °C, for 2010–2011, 2011–2012, and 2012–2013, respectively. Daily average soil temperatures reached a maximum of 20.6 °C (5 cm) and 18.8 °C (20 cm) during the summer of 2010 (Figure 5) but had a weak decreasing trend in the following years, reflecting a trend in decreasing maximum summertime air temperatures and, possibly, a trend in increasing vegetation cover. Due to thick (>0.2 m) snow cover (data not shown) during the winters of 2010–2011 and 2012–2013, there was no soil frost at 5 cm depth during these years. During the winter of 2011–2012, there was no permanent snow cover on any of the plots and the soil froze down to approx. 0.2 m depth. The annual precipitation was lower (487 mm) for the first year than for the following years (610 mm and 611 mm, respectively). On average, soil moisture measured in organic soil, at 5 cm depth, was higher than in the mineral soil, at 20 cm depth.

Figure 5 (panels d and e) suggests that a groundwater table within 20 cm from the soil surface did not result in saturated soil conditions at 20 cm depth in the soil moisture profile. This reflects the difficulties of representing a relatively large area with a highly disturbed soil surface, small-scale variability in topography, differences in soil properties, etc., by measurements at just one location. The groundwater table at the clear-cut was on average approximately 1 m closer to the surface than at the nearby mature forest (Norunda main station, approx. 600 m from the groundwater pipe at plot 2).

The soil surface at the groundwater pipe at the Norunda station was located at 45.5 m a.s.l., while the soil surface at the pipe on plot 2 was located at 49.3 m a.s.l. Thus, since the groundwater pipe in the forest was located 3.8 m lower than the pipe on the clear-cut, it is likely that the higher groundwater levels at the clear-cut were a consequence of the harvest. In general, clear-cutting can be expected to result in a raised groundwater level as a result of decreased canopy interception and evapotranspiration, but the exact magnitude and duration of this increase will depend on, for example, soil properties and vegetation development.

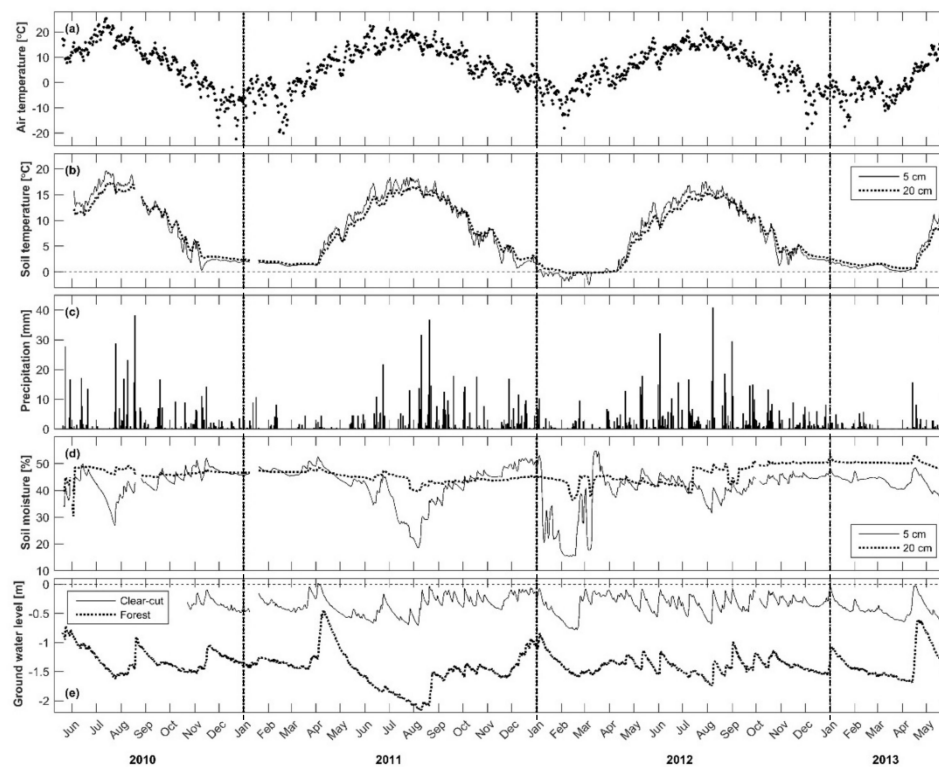


**Figure 5.** Environmental conditions measured at the clear-cut in Norunda from 1 June 2010 to 20 May, 2013. (a) Daily mean air temperature ( $^{\circ}\text{C}$ ) measured at 2 m height at the center of the clear-cut. (b) Daily mean soil temperature ( $^{\circ}\text{C}$ ) at 5 and 20 cm depth, measured at plot 2, close to the edge of plot 1. (c) Daily sum of precipitation (mm), measured at the center of the clear-cut. (d) Daily mean soil moisture (%) at 5 and 20 cm depth, measured at plot 2, close to the edge of plot 1. (e) Daily mean groundwater level at plot 2 and at the nearby mature forest. Vertical dashed lines mark the start of a new year.

During the second half of 2010, it became evident that plot 1 was wetter than plot 2, with several large areas with superficial groundwater. Plot 2 had some small areas with ponds (Figure 3) but was, in general, much drier at the soil surface due to small differences in topography (Figure 2) and possibly due to differences in soil properties (e.g., a clay layer has been found at approx. 1.5 m depth at some locations on both plots but the spatial extent of these layers is unknown). Standing water was often found in soil pits created during soil scarification (approx. 0.3–0.5 m deep) on both plots. The average distances between the calculated groundwater table and the soil surface for October 2010 to May 2013 on plots 1 and 2 (Figure 6) were in good agreement with our qualitative view of the clear-cut, based on field experience, web camera images, etc. In the following, “dry” and “wet” are defined based on the distance from the soil surface to the groundwater table; the closer the groundwater table was to the soil surface, the wetter it was. The driest parts on plot 1 were located East of the tower, i.e., in the least represented wind directions. The wettest parts of plot 2 were in the SSE to NW wind directions, i.e., in the prevailing wind directions. On average, the groundwater table was closer to the surface on

plot 1 than on plot 2 (Figure 7). The daily average distance from the soil surface to the interpolated groundwater table on plots 1 and 2 were 0.16 m and 0.40 m, respectively, for the period October 2010 to May 2013. There was in general a good agreement between groundwater levels calculated for all pipes and the manual measurements (data not shown) when the groundwater level was close ( $> -0.2$  m) to the surface (differences were less than 0.1 m). However, some of the extreme values (calculated groundwater table around 0.2 m above surface) following snowmelt in April 2011 and April 2013 (Figure 7) are likely exaggerated, i.e., in reality, this surface water likely left the area as surface runoff.

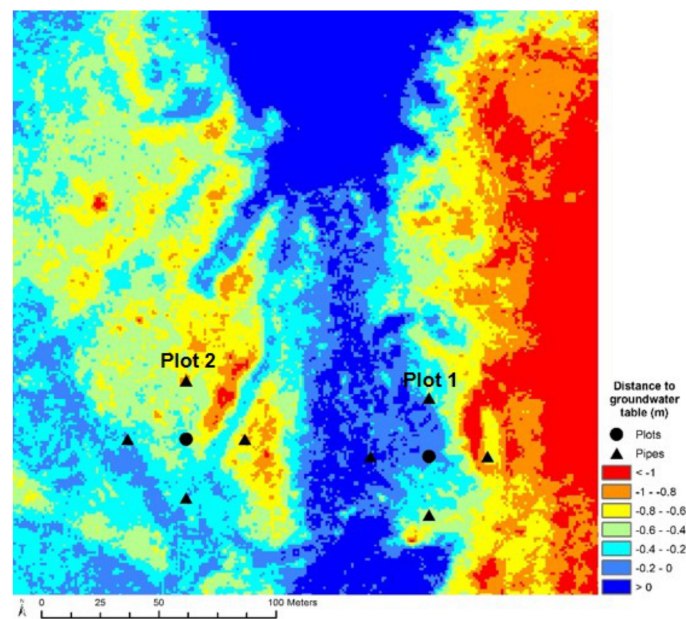


**Figure 6.** Average distances between the soil surface and the interpolated groundwater table for the period October 2010 to May 2013.

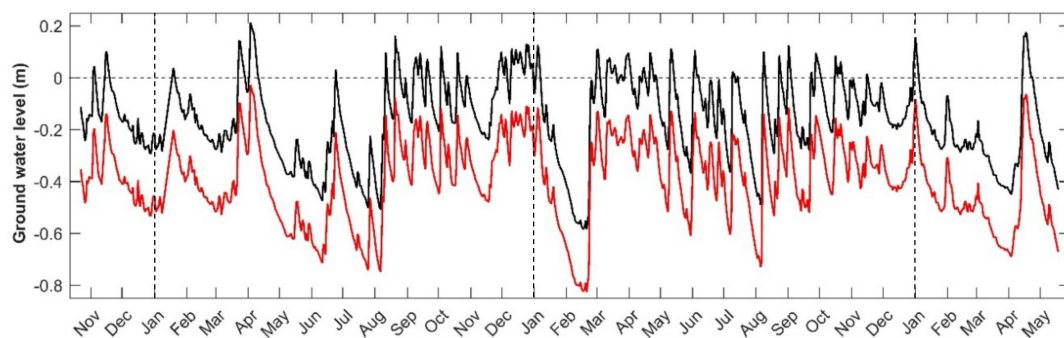


**Figure 7.** Daily average distance between the soil surface and the groundwater table at plot 1 (black line) and plot 2 (red line) from 22 October 2010 to 19 May 2013. Vertical dashed lines mark the start of a new year.

### 3.2. Vegetation Development

The Landsat-derived NDVI for the clear-cut area (Figure 8) suggests that there were no significant differences in vegetation cover on plots 1 and 2 before harvest in early 2009. After harvest, there was a sharp decline in summertime NDVI on both plots followed by a recovery phase until 2012–2013 where NDVI at both plots leveled off at a lower level than before harvest. In 2014, there were no longer any significant differences in NDVI between the plots. The recovery processes at plot 1 were faster and more substantial than on plot 2, indicating a higher vegetation cover from 2009 onwards. During 2009–2011, plot 1 had a significantly higher NDVI ( $p < 0.05$ ) than plot 2. This is also supported

by qualitative information from web cameras (see Figure 3). Given the low survival rate of the seedlings planted in 2010, most of the recovery in the summertime NDVI displayed in Figure 8 was due to the fast establishment of grasses and deciduous shrubs and trees.

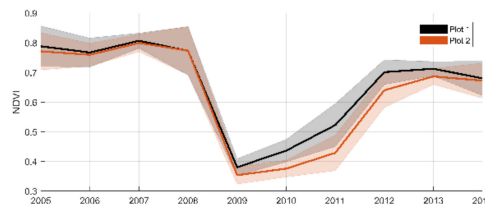


**Figure 8.** Landsat-derived summertime Normalized Difference Vegetation Index (NDVI) from 2005 to 2014, covering both pre- and post-harvest conditions at both plots. The shaded bands represent the standard deviation of the spatially (nine pixels) and temporally (all available Landsat images during the summer (JJA) of each year) averaged data used to create an annual, summertime, NDVI.

### 3.3. Flux Footprints

The areas of plots 1 and 2 were, on average, well represented by the 80% annual flux footprints, despite hourly footprint variation with seasons and years (see Figure 4b for an example from 2012). The footprints were on average larger during nighttime, i.e., partly exceeded the plot area, and, as a result, more nighttime than daytime flux data were removed due to the footprint criteria.

Although the method of Horst [85] does not specifically require horizontally homogeneous fluxes, problems may arise if the concentration footprint of the air intakes at different heights in the towers are fundamentally different at a heavily disturbed clear-cut area. At a small spatial scale (<100 m<sup>2</sup>), the soil and surface conditions were very heterogeneous due to compaction of the soil by the harvester and other heavy machinery, piles of harvest residues and the soil scarification. However, at larger scales (>100 m<sup>2</sup>), surface conditions were more homogenous because most disturbances at the surface were evenly distributed (e.g., mounding was done in a repetitive pattern, harvest residues ended up near the tree stumps). Nonetheless, e.g., wet patches with denser vegetation than on dry patches not seen to the same extent by both air intakes might have contributed to increased uncertainty in the measured fluxes and their source area.

### 3.4. Net Exchange of GHGs

#### 3.4.1. CO<sub>2</sub> Fluxes

The average CO<sub>2</sub> fluxes (filtered for footprint extent; non-gap-filled) during the whole measurement period 2010–2013 were  $-0.3 \mu\text{mol m}^{-2}\text{s}^{-1}$  (plot 1) and  $1.0 \mu\text{mol m}^{-2}\text{s}^{-1}$  (plot 2). The CO<sub>2</sub> fluxes at the two plots differed significantly ( $p < 0.001$ ) for each individual year and for the whole period 2010–2013. On plot 1, the least represented wind directions were from the sector 30°–120°, an area containing some of the drier parts of this plot (Figure 6). However, due to wet conditions and increased vegetation cover in the close vicinity of the tower, there was a net uptake of CO<sub>2</sub> (filtered for footprint extent) in the order of  $-1.2$  to  $-1.5 \mu\text{mol m}^{-2}\text{s}^{-1}$  in this sector. For the remaining sectors, where footprints tended to include wetter areas, average fluxes (per 30° sector) ranged from  $-0.2$  to  $-1.5 \mu\text{mol m}^{-2}\text{s}^{-1}$ . On plot 2, the dominating wind direction was from 120°–240° (i.e., from the relatively wet parts of plot 2, see Figure 9a) but there was no clear dependence of wind direction on the CO<sub>2</sub> fluxes (filtered for footprint extent). Plot 2 was a net source of CO<sub>2</sub> with average net CO<sub>2</sub> emissions of  $0.5$ – $1.8 \mu\text{mol m}^{-2}\text{s}^{-1}$  in the different sectors.

Time series of gap-filled CO<sub>2</sub> data (daily averages, filtered according to footprint classification) are shown in Figure 9a. Initially, there was little vegetation on any of the plots and respiration dominated but already by the end of the first growing season, there were days with net uptake of CO<sub>2</sub> at plot 1. During the growing seasons of 2011 and 2012, the net uptake at plot 1 peaked in July, but by August, the fluxes were positive again. These early and short periods of net uptakes highlight the importance of

grasses on clear-cuts for the CO<sub>2</sub> budget. The sudden shift in CO<sub>2</sub> fluxes on plot 1 in January 2013 was related to a raised groundwater table and increased soil moisture that possibly limited heterotrophic respiration and/or gross photosynthesis. Apart from a short period in June–July 2012, there were only daily average net emissions of CO<sub>2</sub> on plot 2, i.e., plot 2 was on a daily basis a source of CO<sub>2</sub>. Averaged over the whole period 2010–2013, the net emissions were 0.5  $\mu\text{mol m}^{-2}\text{s}^{-1}$  (plot 1) and 1.1  $\mu\text{mol m}^{-2}\text{s}^{-1}$  (plot 2), respectively. The cumulative CO<sub>2</sub> fluxes 2010–2013 were 3773 gCO<sub>2</sub> m<sup>-2</sup> and 5181 gCO<sub>2</sub> m<sup>-2</sup> on plots 1 and 2, respectively (Table 2).

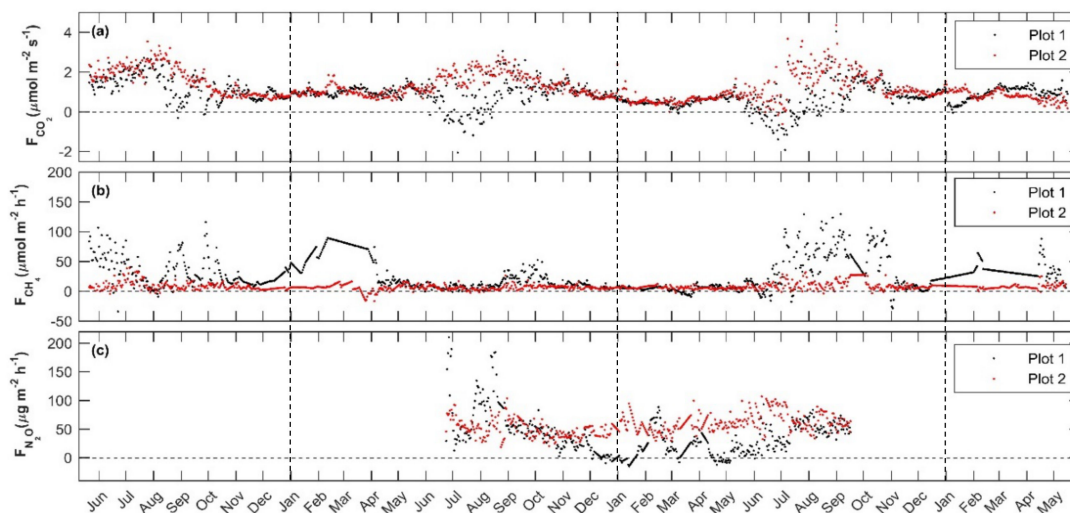


**Figure 9.** Daily average Greenhouse Gas (GHG) fluxes at plot 1 (black dots) and plot 2 (red dots). (a) CO<sub>2</sub> fluxes from May 2010 to May 2013. (b) CH<sub>4</sub> fluxes from May 2010 to May 2013. (c) N<sub>2</sub>O fluxes from June 2011 to September 2012. The effect of gap-filling using linear interpolation can be clearly seen in, e.g., February–April 2011 (panel b) and in, e.g., January 2012 (panel c). Vertical dashed lines mark the start of a new year.

**Table 2.** Cumulative GHG fluxes from May 2010 to May 2011 (year 1), May 2011–May 2012 (year 2) and May 2012 to May 2013 (year 3). The global warming potential factors used in the conversions for gCH<sub>4</sub> m<sup>-2</sup> and gN<sub>2</sub>O m<sup>-2</sup> were 28 and 265, respectively [91].

Plot	Year	NEE (gCO <sub>2</sub> m <sup>-2</sup> )	R <sub>eco</sub> (gCO <sub>2</sub> m <sup>-2</sup> )	GPP (gCO <sub>2</sub> m <sup>-2</sup> )	CH <sub>4</sub> (gCO <sub>2</sub> -eq m <sup>-2</sup> )	N <sub>2</sub> O (gCO <sub>2</sub> -eq m <sup>-2</sup> )	GHG Budget (gCO <sub>2</sub> -eq m <sup>-2</sup> )
Plot 1	1	1607.9	2287.8	-679.9	153.1	-	1761.0 *
Plot 2	1	1911.2	2083.1	-171.9	30.3	-	1941.5 *
Plot 1	2	1052.5	2507.8	-1455.3	37.6	78.2	1168.3 **
Plot 2	2	1645.0	2152.8	-507.8	25.3	111.9	1782.2 **
Plot 1	3	1112.7	2589.7	-1477.0	143.1	32.5	1288.3 **
Plot 2	3	1624.7	2556.3	-931.6	37.9	52.2	1714.8 **
Plot 1	1–3	3773.1	7385.3	-3612.1	333.8	110.7	4217.6
Plot 2	1–3	5180.8	6792.1	-1611.3	93.5	164.1	5438.4
Plot 1	***	952.7	2456.5	-1503.8	39.3	77.9	1069.9
Plot 2	***	1541.0	2174.8	-633.8	25.8	128.8	1695.7

\* N<sub>2</sub>O fluxes were not measured during Year 1. \*\* Note that the contribution of N<sub>2</sub>O to the full GHG budget is based on 11 months of data in year 2 and on only 4 months in year 3. \*\*\* Year is here defined as 1 July 2011 to 30 June 2012, to make possible a direct comparison of the importance of the different GHGs.

The difference in cumulative ecosystem respiration ( $R_{eco}$ ) between the plots was relatively small (~600 gCO<sub>2</sub> m<sup>-2</sup> for the three-year period), with the highest  $R_{eco}$  on plot 1 (Figure 10). The lower (~1400 gCO<sub>2</sub> m<sup>-2</sup>) net emissions of CO<sub>2</sub> on plot 1 can be fully explained by higher  $GPP$  (~2000 gCO<sub>2</sub> m<sup>-2</sup>), which again highlights the importance of the fast establishment of grasses and shrubs on the total CO<sub>2</sub> budget. See Figure 10 for details on  $R_{eco}$  and  $GPP$  during the individual years.

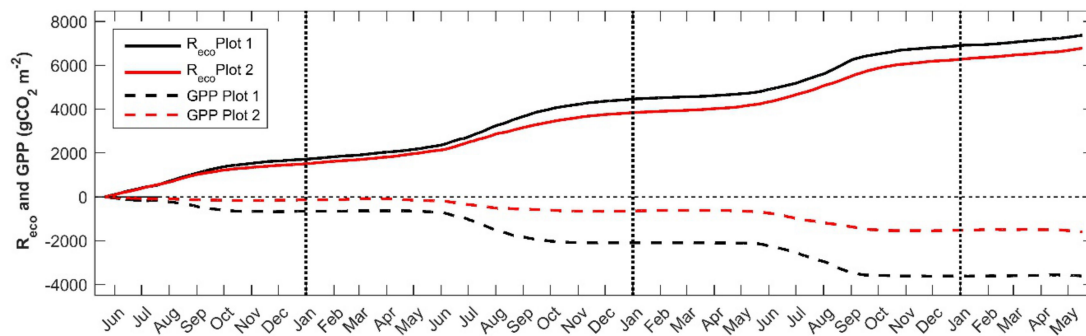


**Figure 10.** Ecosystem respiration and Gross Primary Productivity ( $GPP$ ) in  $gCO_2 m^{-2}$  from May 2010 through May 2013 on plot 1 ( $R_{eco}$ —black line,  $GPP$ —black dashed line) and plot 2 ( $R_{eco}$ —red line,  $GPP$ —red dashed line). Vertical dashed lines mark the start of a new year.

### 3.4.2. $CH_4$ Fluxes

The average  $CH_4$  fluxes (filtered for footprint extent; non-gap-filled) for the whole period 2010–2013 were  $26.1 \mu mol m^{-2}h^{-1}$  and  $8.2 \mu mol m^{-2}h^{-1}$  on plots 1 and 2, respectively. The fluxes at the two plots differed significantly ( $p < 0.001$ ) for the whole period and, with the exception of May 2011–May 2012, for the individual years. The net average emissions (per  $30^\circ$  sector) of  $CH_4$  on plot 1 (filtered for footprint extent) ranged between  $15.9$ – $38.0 \mu mol m^{-2}h^{-1}$ , with the lowest emission ( $15.9 \mu mol m^{-2}h^{-1}$ ) from footprints originating from the most represented wind sector  $150^\circ$ – $180^\circ$  on plot 1. The estimation of the groundwater surfaces suggests that this was a relatively dry part of plot 1 (Figure 6). The highest average emissions ( $31.7$ – $38.0 \mu mol m^{-2}h^{-1}$ ) originated from footprints with wind directions  $270^\circ$ – $90^\circ$ , which included many wet and dry parts (Figure 6). On plot 2, there was no clear dependence of wind direction on the average  $CH_4$  fluxes although  $CH_4$  emissions were slightly higher ( $10.4$ – $12.4 \mu mol m^{-2}h^{-1}$ ) for footprints with wind directions from  $60^\circ$ – $180^\circ$  than from other sectors ( $4.7$ – $9.2 \mu mol m^{-2}h^{-1}$ ).

Time series of daily average, gap-filled  $CH_4$  fluxes (filtered for footprint classification) are shown in Figure 9b. Apart from a few periods with net  $CH_4$  consumption, both plots were net sources of  $CH_4$ . Plot 2 had relatively low and stable net emissions throughout the measurement period, while the  $CH_4$  emissions at plot 1 were higher and more variable. During the first year of measurements, the net emissions of  $CH_4$  were considerably higher on plot 1 than on plot 2, and there were several peaks (e.g., in August–September and in October) that coincided with precipitation events and peaks in soil moisture at 20 cm depth (Figure 5). With the exception of emission peaks on plot 1 in August–October 2011, the  $CH_4$  exchanges were low and similar on both plots following snowmelt in 2011 until June 2012 where net emissions increased considerably on plot 1. Average fluxes based on the footprint classification were  $22.6 \mu mol m^{-2}h^{-1}$  and  $8.2 \mu mol m^{-2}h^{-1}$  on plots 1 and 2, respectively.

### 3.4.3. $N_2O$ Fluxes

The average  $N_2O$  fluxes (filtered for footprint extent; non-gap-filled) during the whole measurement period June 2011–September 2012 were  $47.4 \mu g m^{-2}h^{-1}$  and  $64.9 \mu g m^{-2}h^{-1}$  on plots 1 and 2, respectively. The  $N_2O$  fluxes at plots 1 and 2 were significantly different ( $p < 0.001$ ). The lowest average (per  $30^\circ$  sector)  $N_2O$  fluxes (filtered for footprint extent) on plot 1 ( $33.0$ – $38.4 \mu g m^{-2}h^{-1}$ ) came from footprints originating from the least represented wind directions ( $30^\circ$ – $120^\circ$ ), and included some of the drier parts of plot 1, i.e., areas with the largest distance from the soil surface to the groundwater table (Figure 6). For footprints originating from all other wind sectors, the average  $N_2O$  fluxes ranged between  $41.8$ – $57.7 \mu g m^{-2}h^{-1}$ . On plot 2, there was no clear dependence of wind direction on average  $N_2O$  fluxes. The  $N_2O$  emissions ranged between  $49.3$ – $75.2 \mu g m^{-2}h^{-1}$ , with the highest emissions from the drier sectors  $330^\circ$ – $90^\circ$ .

Time series of daily average, gap-filled  $N_2O$  fluxes (filtered for footprint classification) are shown in Figure 9c. The highest net emissions (up to  $\sim 200 \mu g m^{-2}h^{-1}$ ) were on plot 1 during the summer of

2011, a relatively dry period with a few precipitation events causing large variations in groundwater level and soil moisture (especially at 20 cm depth). During December 2011 through mid-January 2012, wetter conditions were observed in general (at both 5 and 20 cm depth) and the groundwater table was often close to the surface. During this time, there was a small net uptake of N<sub>2</sub>O in the order of 5–10 µgm<sup>-2</sup>h<sup>-1</sup> on plot 1. The uptake period ended when the soil froze in mid-January 2012, and was instead turned into an emission peak that lasted for more than a month. During this period, soil moisture dropped rapidly when the soil froze and there was a decreasing trend in groundwater level. The N<sub>2</sub>O emissions started to decrease again in the middle of February when soil temperature was close to 0 °C and soil moisture levels and groundwater levels increased again. This was followed by a second emission peak at the beginning of March when the soil froze again. There was a second period with net N<sub>2</sub>O uptake during the latter half of April 2012, when soil temperature was above 0 °C again, the soil was wet and the groundwater level was close to the surface.

The net N<sub>2</sub>O emissions on plot 2 were generally higher than on plot 1, and also had a less variable temporal pattern. There were no periods with net uptake of N<sub>2</sub>O on the drier plot 2. The average N<sub>2</sub>O fluxes, based on the larger surface area specified by the footprint classification (Figure 4b) were 37.4 and 57.5 µg m<sup>-2</sup>h<sup>-1</sup> on plots 1 and 2, respectively. The cumulative fluxes for a full year of N<sub>2</sub>O measurements (1 July 2011 through 30 June 2012) were 0.29 gN<sub>2</sub>O m<sup>-2</sup> (plot 1) and 0.49 gN<sub>2</sub>O m<sup>-2</sup> (plot 2).

### 3.5. Diel Patterns of CO<sub>2</sub>, CH<sub>4</sub> and N<sub>2</sub>O Fluxes

There were clear mean diel patterns in the CO<sub>2</sub> exchange during summer (JJA) on both plots, except for the first year on plot 2 (Figure 11, top panel), with a clear trend towards higher uptake with time. The diel patterns were also visible during the fall (SON), but not during winter (DJF) or spring (MAM). The net uptake was largest on plot 1 during the summer of 2012 where the mean uptake at noon reached almost 4 µmol m<sup>-2</sup>s<sup>-1</sup>. The trend towards larger uptake reflects the establishment of opportunistic pioneer species (mainly grasses and shrubs) and eventually, also the growth of the planted seedlings.

There were no clear mean diel patterns in CH<sub>4</sub> exchange on the drier plot 2, in any season or year (Figure 11, middle panel). On the wetter plot 1, the picture was more complex with, in general, higher net emissions and seasons without any clear mean diel patterns (e.g., DJF all years, MAM in 2011–2012, JJA in 2011), periods with clear diel curves with amplitudes in the order of ~10–20 µmol m<sup>-2</sup>h<sup>-1</sup> (JJA in 2010 and 2012 and SON in 2012) as well as periods with a weak tendency of a diel pattern (MAM in 2010 and SON 2010–2011). Spring 2010 sticks out with the highest emissions and an irregularly shaped diel curve, but since measurements of CH<sub>4</sub> started 20 May 2010, it is based on only 11 days of data collected directly after the mounding and planting and cannot be regarded as representative of the whole MAM period in 2010. Nonetheless, the scarcity of data on ecosystem CH<sub>4</sub> fluxes directly following a severe disturbance in a hemiboreal forest justifies the inclusion of this period in the analysis.

There were clear diel patterns in the N<sub>2</sub>O exchange on plot 1 during JJA and SON in both 2011 and 2012, with the largest diel amplitude (daytime maxima) in JJA 2011 and SON 2012 (~35 µg m<sup>-2</sup>h<sup>-1</sup>) (Figure 11, lower panel). The 2012 SON curve is based on less than a month of data and is thus not representative of the whole SON period, but is still interesting due to the scarcity of measurements of ecosystem N<sub>2</sub>O fluxes in managed forest ecosystems. There was a weak tendency towards larger diel variability in N<sub>2</sub>O exchange during periods with higher net N<sub>2</sub>O emissions and lower diel variations during periods with lower net emissions, or even net uptake (see Figure 9c). On the other hand, these low-emission periods were also characterized by emission peaks in February 2012 and in March–April 2012. In plot 2, there were no clear diel trends in N<sub>2</sub>O exchange during JJA and SON 2011 and DJF 2012, and clear daytime maxima (amplitude of the diel curve was in the order of 20–35 µg m<sup>-2</sup>h<sup>-1</sup>) during MAM, JJA and SON 2012. Hence, on plot 2, there was no clear tendency towards larger diel variability with higher net emissions of N<sub>2</sub>O.

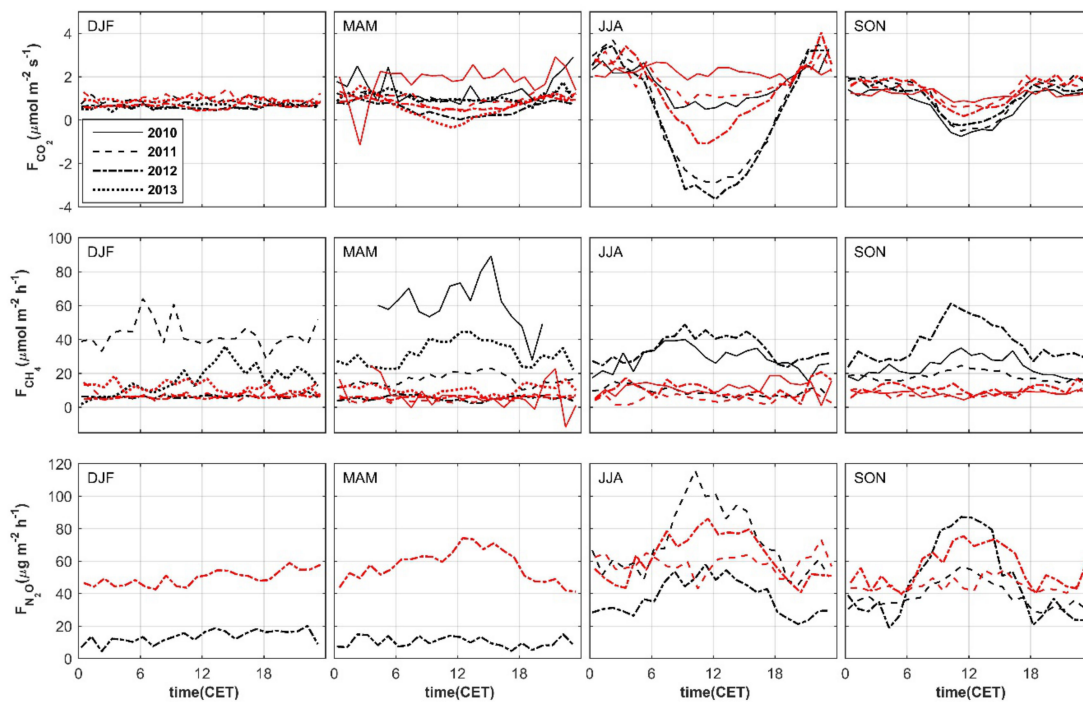


**Figure 11.** Mean diel GHG exchanges during the winter (DJF), spring (MAM), summer (JJA) and fall (SON) seasons of 2010 to 2013. Black lines represent fluxes at plot 1, while red lines represent fluxes at plot 2. Top panel: CO<sub>2</sub> fluxes; Middle panel: CH<sub>4</sub> fluxes. Lower panel: N<sub>2</sub>O fluxes. Note that the CH<sub>4</sub> fluxes during MAM 2010 are based on only 11 days of data in May and that the N<sub>2</sub>O fluxes during SON 2012 are based on only 27 days of data in September.

#### Total GHG Budgets

In order to compare the relative importance of the different GHGs, cumulative sums of gap-filled CH<sub>4</sub> and N<sub>2</sub>O fluxes were converted into grams of CO<sub>2</sub>-equivalents per square meter (in a 100-year-perspective). As shown in Table 2, the annual net CO<sub>2</sub> emissions were consistently lower on plot 1 than on plot 2, but this was partly offset by higher CH<sub>4</sub> emissions, especially during 2010–2011 and 2012–2013. During 2011–2012, N<sub>2</sub>O emissions contributed more to the total GHG budget on both plots than CH<sub>4</sub> emissions did, despite that N<sub>2</sub>O exchanges were only measured during 11 months this year.

The total net CO<sub>2</sub> and CH<sub>4</sub> emissions over three years were approx. 4107 gCO<sub>2</sub>-eq m<sup>-2</sup> and 5274 gCO<sub>2</sub>-eq m<sup>-2</sup> on plots 1 and 2, respectively. Carbon dioxide contributed 91.8% (plot 1) and 98.2% (plot 2) to the total CO<sub>2</sub> budget. Unfortunately, due to technical problems, the N<sub>2</sub>O fluxes were not measured for the full 36-month period, making it impossible to derive a full GHG budget for the whole period. In Table 2, we have added the contribution of N<sub>2</sub>O during the periods it was measured in the individual years. Despite the shorter measurement periods of N<sub>2</sub>O fluxes in the individual years, N<sub>2</sub>O still contributed significantly to the total GHG budget for these periods. To make it possible to directly compare the relative importance of the GHGs, we also compiled a total GHG budget for a full year, defined as 1 July 2011 to 30 June 2012 (see \*\*\* in Table 2), with simultaneous measurements of all GHGs. On plot 1, CH<sub>4</sub> and N<sub>2</sub>O contributed with 3.7% (39.3 gCO<sub>2</sub>-eq m<sup>-2</sup>) and 7.3% (77.9 gCO<sub>2</sub>-eq m<sup>-2</sup>), respectively, to the total GHG budget. On plot 2, CH<sub>4</sub> fluxes contributed with 1.5% (25.8 gCO<sub>2</sub>-eq m<sup>-2</sup>) while N<sub>2</sub>O fluxes contributed with 7.6% (128.8 gCO<sub>2</sub>-eq m<sup>-2</sup>) to the GHG budget.

#### 4. Discussion

The results show that clear-cutting of a hemiboreal forest stand resulted in large GHG emissions over the first three years and that the relative contribution of the three GHGs in the total GHG budget

depended on the degree of wetness of the plots. The clear-cutting resulted in waterlogged soils, which most likely caused the site to switch from a sink to a source of CH<sub>4</sub>. N<sub>2</sub>O fluxes contributed more to the total GHG budget than CH<sub>4</sub> fluxes did, even on the wet plot 1 where occasional net uptake of N<sub>2</sub>O was found.

#### 4.1. Vegetation Development

The vegetation development had a large impact on CO<sub>2</sub> fluxes at both plots. While the ecosystem respiration was similar at both plots, the higher GPP (due to higher vegetation coverage) at plot 1 resulted in lower total net emissions than at the drier plot 2. This observation was also supported by both the summertime NDVI data (Figure 8) and by the differences in the temporal evolution of the diel curves in CO<sub>2</sub> fluxes (Figure 11) on plots 1 and 2. Given the low survival rate of the seedlings planted in May 2010, it was evident that a large part of the differences in GPP between the plots could be explained by the faster and more substantial establishment of grasses and shrubs at the wetter plot 1. Even though GPP increased 5.4-fold from year 1 to year 3 on plot 2, it was consistently lower than at plot 1, where GPP only increased by a factor of ~2.2—from the period 2010–2011 to 2012–2013. The recovery rate in GPP on plot 1 is similar to values reported by Williams, Vanderhoof [44] (a 1.7-fold increase in summertime GPP over the first three years after clear-cutting of mixed spruce and deciduous hardwood forest in northeastern US) and Humphreys, Andrew Black [40] (a 2.9-fold increase in annual GPP over the first three years following clear-cutting of a Douglas-fir stand in western Canada).

#### 4.2. Gap-Filling of CH<sub>4</sub> and N<sub>2</sub>O Fluxes

In order to derive a full GHG balance, gap-free data of high quality are required. Well-established gap-filling methods for times series of CO<sub>2</sub> fluxes exist; however, there is currently no general consensus on gap-filling of CH<sub>4</sub> and N<sub>2</sub>O fluxes. Attempts have been made to fill gaps in CH<sub>4</sub> fluxes of wetlands using, e.g., temperature relationships, simple linear interpolation and neural networks [95–97]. Sundqvist, Persson [98] described an empirical model based on multiple stepwise regression analysis for upscaling methane exchange from point measurements (chambers) to the stand scale at the Norunda forest using relationships between CH<sub>4</sub> fluxes and soil temperature, soil moisture and water table depth. It was not possible to find any similar relationships between CH<sub>4</sub> exchange and typical controlling variables on the clear-cut plots 1 and 2, most likely due to the heavily disturbed soil and changes in hydrology following harvest, and hence, we filled gaps using linear interpolation of daily average CH<sub>4</sub> fluxes.

N<sub>2</sub>O fluxes are notoriously variable, both temporally and spatially, making gap-filling even more complex than for CH<sub>4</sub>. Scanlon and Kiely [90] used linear interpolation of daily average fluxes to fill gaps in N<sub>2</sub>O fluxes (EC) at a managed grassland, while Mishurov and Kiely [99] tested linear extrapolation, moving average and a look-up table approach to fill gaps of different lengths (day, month and year) in the same ecosystem. In total, six methods were tested by the authors and they were found to agree reasonably well. Additionally, Merbold, Eugster [31] filled gaps in N<sub>2</sub>O fluxes at a managed grassland using look-up tables for periods with similar environmental conditions. For our highly disturbed ecosystem with large temporal and spatial variability in known controlling parameters, and poor spatial representation of, e.g., soil moisture and soil temperature measurements, the simpler linear interpolation method was chosen.

#### 4.3. Diel Patterns of CH<sub>4</sub> and N<sub>2</sub>O Fluxes

The absence of clear diel variations in CH<sub>4</sub> exchange at the drier plot 2 was probably a consequence of the, on average, larger distance from the soil surface to the groundwater, which resulted in lower CH<sub>4</sub> production rates. In addition, the highly disturbed soil surface is likely to have reduced CH<sub>4</sub> consumption, as compared to undisturbed soil. Teepe, Brumme [100] and Strömngren, Hedwall [28] showed decreased CH<sub>4</sub> consumption, and even net CH<sub>4</sub> emissions, from wheel ruts on clear-cuts, probably as a consequence of reduced macropore volume due to compaction, which limited diffusion

of atmospheric CH<sub>4</sub> into the soils. Other studies have shown that it takes years [101] to more than a century [9] for disturbed soils to regain their full sink capacity.

There were either clear or weak diel variations in CH<sub>4</sub> exchange on the wetter plot 1 during all seasons, but the amplitude varied between seasons and years. Given that methanogens normally have a higher temperature sensitivity than methanotrophs [102], it is possible that the high groundwater level and the severely disturbed soil surface (i.e., high production rates and low consumption rates) can explain the observed diel patterns with daytime maxima in CH<sub>4</sub> exchange. On the other hand, we found no, or only very weak, correlations between soil temperature (at any depth) and CH<sub>4</sub> fluxes at any of the plots. However, this might be a result of the poor spatial representation of soil temperature measurements at the clear-cut. The absence of a diel pattern on plot 1 during JJA in 2011 was probably related to the lower than average groundwater level during this period.

A few studies have reported diel patterns of CH<sub>4</sub> exchange in forest ecosystems. Pattey, Strachan [48] reported daytime maxima of CH<sub>4</sub> emissions over a boreal forest, using both flux-gradient and EC techniques during shorter campaigns, and noted that the CH<sub>4</sub> cycle closely followed the soil temperature cycle at 5 cm depth. Other studies have reported daytime minima [49,103] in CH<sub>4</sub> fluxes. Sundqvist, Mölder [104] measured CH<sub>4</sub> fluxes in the Norunda forest with different gradient methods above the canopy and suggested that the observed daytime minima could be a result of plant uptake (as previously observed from branch chamber measurements by Sundqvist, Crill [105]) and that the observed nighttime maxima could be a result of larger nighttime footprints, with distant, wetter source areas (such as the clear-cut in this study) contributing more to the measured fluxes than during daytime.

Diel patterns of N<sub>2</sub>O fluxes from agricultural soils and grasslands have been known for about 40 years [106–108]. Recently, Shurpali, Rannik [109] reported clear diurnal variability in N<sub>2</sub>O fluxes (measured with EC on agricultural land) depending on soil N availability. They attributed daytime flux maxima during high soil N availability (i.e., following fertilization) to soil temperature control on the involved microbial processes, while the N<sub>2</sub>O fluxes during low soil N availability correlated negatively with GPP. Their study suggests that plants play a role in the N<sub>2</sub>O exchange by moderating soil O<sub>2</sub> levels in the soil and nitrogen availability (either directly through plant uptake of nitrogen or indirectly through root exudates of carbon that stimulates immobilization of inorganic nitrogen by heterotrophic bacteria). The net result would be reduced N<sub>2</sub>O production and increased reduction of N<sub>2</sub>O to N<sub>2</sub> and hence, reduced net emissions or even net uptake of N<sub>2</sub>O. Our results are different from those of Shurpali, Rannik [109], i.e., with clear daytime maxima of the N<sub>2</sub>O exchange during seasons when GPP was at its maximum, and during what would be considered as a low-flux period in the study of Shurpali, Rannik [109]. During seasons with no or low diel amplitude of the diel CO<sub>2</sub> exchange (DJF, MAM), the amplitude of the diel N<sub>2</sub>O exchange was also non-existent or low. During seasons with larger diel amplitudes in CO<sub>2</sub> fluxes (JJA, SON), the diel amplitude in N<sub>2</sub>O fluxes was also higher. Furthermore, the magnitude of the flux seemed to have an impact on the amplitude of the diel curves; the lower the flux, the lower the amplitude. Zona, Janssens [110] measured EC N<sub>2</sub>O fluxes above a short-rotation poplar plantation and found no diurnal patterns in the fluxes except during shorter periods. The controlling factor of the diurnal pattern during these short periods was found to be wind speed.

Unfortunately, we do not have any data on soil O<sub>2</sub> concentrations or on available soil N that could explain our observed diel patterns at plots 1 and 2. However, it is likely that with flux footprints integrating fluxes from a heavily disturbed ecosystem with small-scale variability in topography, soil moisture, soil temperature, distance to the groundwater table, soil properties, pH, available soil N, etc., hence encompassing a wide range of environmental, biogeochemical and biogeophysical conditions, it is difficult, if not impossible, to draw any conclusions on the key drivers of the observed diel patterns.

We are not aware of any micrometeorological studies of N<sub>2</sub>O fluxes at clear-cut forest stands.

#### 4.4. Greenhouse Gas Fluxes

Our approach, applying a very strict filtering based on footprint extent (and on turbulence parameters, etc.) of the flux data resulted in a much reduced dataset and in a strong confidence that the remaining fluxes were representative for plots 1 and 2, respectively. By applying a statistical test (Wilcoxon signed-rank test for zero median) on pairwise data (fluxes measured during the same hour) from plots 1 and 2, robust and statistically significant differences in fluxes of CO<sub>2</sub>, CH<sub>4</sub> and N<sub>2</sub>O were observed. We mainly attribute the differences in fluxes to differences in the wetness at the plots, either directly (e.g., through the effect of the groundwater table position on fluxes of CH<sub>4</sub> and N<sub>2</sub>O) or indirectly, through the faster and more substantial establishment of vegetation on the wetter plot 1 (and especially around ponds and other wetter areas at plot 1), which had a significant impact on the net emissions of CO<sub>2</sub>. As a consequence of the very strict data filtering on footprint extent, a large proportion of nighttime and wintertime data was lost and hence, the non-gap-filled CO<sub>2</sub> fluxes were biased towards net uptake of CO<sub>2</sub> (plot 1) or smaller net emissions (plot 2).

The less strict filtering on footprint classification, and the subsequent gap-filling, made it possible to derive annual cumulative sums of NEE, GPP and R<sub>eco</sub> for plots 1 and 2. The values for the first three years after clear-cutting reported here (Table 2) were lower than those reported after clear-cutting of Douglas fir stands in Western Canada Humphreys, Andrew Black [40] and Paul-Limoges, Black [45] reported total net emissions of CO<sub>2</sub> of ~6380 gCO<sub>2</sub>m<sup>-2</sup> and ~8900 gCO<sub>2</sub>m<sup>-2</sup>, respectively). Additionally, Korkiakoski, Tuovinen [15] reported higher net emissions from a drained peatland in Finland for the first two years following clear-cutting of a Scots pine-dominated stand (~3090 gCO<sub>2</sub>m<sup>-2</sup> and ~2070 gCO<sub>2</sub>m<sup>-2</sup> for year 1 and 2, respectively). Our net CO<sub>2</sub> emissions reported here are higher than those reported by Coursolle, Giasson [43] (net emissions of ~1550 gCO<sub>2</sub>m<sup>-2</sup> the first three years after clear-cutting of a Black spruce (*Picea mariana*) in eastern Canada). Amiro, Barr [33] reported annual net emissions of CO<sub>2</sub> in the order of 730–3120 gCO<sub>2</sub>m<sup>-2</sup> following clear-cutting of a wide range of forest across North America, with boreal forests being in the lower end of that range.

Similar to Amiro, Barr [33] and Williams, Vanderhoof [44], we observed relatively stable R<sub>eco</sub> for the years following clear-cutting and a gradual recovery in GPP, which further stresses the importance of vegetation development for the carbon balance of a clear-cut forest stand.

We do not have any pre-harvest measurements of CH<sub>4</sub> fluxes at our clear-cut but simultaneous chamber measurements in an undisturbed forest in the close vicinity of the Norunda station and on plot 2 at the clear-cut by Sundqvist, Vestin [14] showed net uptake in the order of −10 μmol m<sup>-1</sup>h<sup>-1</sup> in the undisturbed forest and average net CH<sub>4</sub> emissions of 13.6 μmol m<sup>-1</sup>h<sup>-1</sup> on plot 2 in October–November 2010. The results from plot 2 were in good agreement with our flux-gradient CH<sub>4</sub> measurements during the same period. Sundqvist, Vestin [14] used an automated chamber system with five chambers placed on both disturbed and undisturbed soil on plot 2 and found net emissions in the order of 15–32.5 μmol m<sup>-1</sup>h<sup>-1</sup> from chambers placed on disturbed soil and either small net emissions or small net uptake (−3 μmol m<sup>-1</sup>h<sup>-1</sup>) from chambers placed on undisturbed soil. The distance from the chamber frame to the groundwater table was 0.44–0.5 m for the chamber with net uptake, while the distances were less than 0.21 m for chambers with net emissions. Most chambers were placed southwest of the tower on plot 2, i.e., at the wetter parts of plot 2 (Figure 6). The average distances to the groundwater table were 0.16 m and 0.40 m on plots 1 and 2, respectively, which most likely explains the observed differences in CH<sub>4</sub> emissions between the plots. Furthermore, our observations during the period 2010–2013 support the initial observation by Sundqvist, Vestin [14] in 2010 that waterlogging following clear-cutting caused the site to switch from a sink to a source of CH<sub>4</sub>. Others have also reported how a site switched from a sink to a source following clear-cutting, either as a result of increased soil moisture that inhibited CH<sub>4</sub> consumption [13], a higher water table [15] or as the combined result of increased soil moisture, higher water table and increased soil N availability [16].

Our results with high and variable CH<sub>4</sub> emissions (plot 1) or low and steady emissions (plot 2) are different from results reported by Strömngren, Hedwall [28], who used chambers to measure fluxes from soils disturbed by soil preparation and wheel ruts in three clear-cut Norway spruce forests in

central Sweden. The authors found reduced uptake rates of CH<sub>4</sub> at soil pits and large emissions from wheel ruts, as compared to control plots with undisturbed soils. However, when scaled to stand level according to the area coverage by each disturbance type, they found no significant differences between control plots and treated plots. Similarly, Kulmala, Aaltonen [68] found no significant difference in CH<sub>4</sub> fluxes between a mature forest and a clear-cut plot in a chamber study at a Norway spruce forest in southern Finland. The soil at the clear-cut remained a sink throughout the three-year study period.

The net fluxes of N<sub>2</sub>O at plot 1 were highly variable, ranging from a small net uptake (December 2011–January 2012 and April–May 2012) to large emission peaks (e.g., JJA 2011, February 2012 and March–April 2012). It seems likely that the emission peaks in JJA 2011 were caused by precipitation events and related fluctuations in soil moisture and groundwater table depth and that the emission peaks in February 2012 and March–April 2012 was related to freezing and thawing of the soil at plot 1. N<sub>2</sub>O fluxes are known to be highly variable in space and time and many have reported that a single, or a few, emission events following, e.g., fertilization [111], precipitation events [110], or freeze–thaw events [112], can make up a large portion of the annual N<sub>2</sub>O budget. The N<sub>2</sub>O fluxes at plot 2 were generally higher and less variable than at plot 1. There were no clear effects of precipitation events and freeze–thaw cycles at plot 2, possibly because of the lower groundwater table.

The small net uptake of N<sub>2</sub>O we observed at the wet plot 1 is similar to previously reported EC values for forests [24,25,53] and for chamber measurements in the forest [112] and in clear-cut boreal forests [27,28].

#### 4.5. GHG Budgets

For the only full year with simultaneous measurements of all GHGs (1 July 2011 to 30 June 2012), CO<sub>2</sub> contributed 89.0% and 90.9% to the total GHG budget on plots 1 and 2, respectively. The contribution of CH<sub>4</sub> to the total budget was low during this year, possibly as a consequence of the lower than average groundwater table position (during July and August in 2011 and during January and February 2012) and because of soil frost during the snow-free winter 2011–2012. The contribution of N<sub>2</sub>O to total GHG emissions was 7.3% and 7.6% on plots 1 and 2, respectively, although the N<sub>2</sub>O emissions at the drier plot 2 were 65% higher in absolute terms than at the wetter plot 1.

The total GHG budget was lower (plot 1) and higher (plot 2) than values reported (1581 gCO<sub>2</sub>-eq.m<sup>-2</sup> with GWP<sub>100</sub> factors of 23 and 296 for CH<sub>4</sub> and N<sub>2</sub>O, respectively) for a chamber study during the first ten months following clear-cutting of a Sitka spruce plantation in Northern England [16]. Zona, Janssens [54] reported a net uptake of CO<sub>2</sub> of −76 gCO<sub>2</sub>-eq.m<sup>-2</sup> and a combined net release of 351 gCO<sub>2</sub>-eq.m<sup>-2</sup> for CH<sub>4</sub> and N<sub>2</sub>O (using GWP<sub>100</sub> factors of 25 and 298 for CH<sub>4</sub> and N<sub>2</sub>O, respectively) during a one and a half year study period at a short-rotation bioenergy poplar plantation in Belgium. In their study, water availability was the main driver of CO<sub>2</sub> uptake and CH<sub>4</sub> and N<sub>2</sub>O emissions. Peichl, Arain [32] combined EC measurements of CO<sub>2</sub> (mean value over a four year study period) with chamber measurements of CH<sub>4</sub> and N<sub>2</sub>O (mean value over two years) in a White pine (*Pinus strobus*) stand that was seven years old at the start of the measurements. As in our study, CO<sub>2</sub> fluxes were the main contributor to the total GHG budget, while CH<sub>4</sub> and N<sub>2</sub>O fluxes combined contributed 13%. Korkiakoski, Tuovinen [15] also used a combination of EC measurements of CO<sub>2</sub> with manual chamber measurements of CH<sub>4</sub> and N<sub>2</sub>O at a clear-cut forest on a nutrient-rich drained peatland and noted a switch from a weak CH<sub>4</sub> sink to a weak CH<sub>4</sub> source and from N<sub>2</sub>O neutral into a significant N<sub>2</sub>O source. While the CO<sub>2</sub> emissions were large, the CH<sub>4</sub> emissions were deemed negligible in a global warming potential perspective (GWP<sub>100</sub> = 34) and the N<sub>2</sub>O contribution was in the order of 10% (GWP<sub>100</sub> = 298) of the CO<sub>2</sub> fluxes, i.e., very similar to our study.

At plot 2, CH<sub>4</sub> emissions were relatively low and constant during the study period (Table 2), while the net emissions were much lower at plot 1 during 2011–2012, which to a large part overlaps with the year used for creating full GHG budgets (see Table 2). During the periods 2010–2011 and 2012–2013, CH<sub>4</sub> fluxes (in gCO<sub>2</sub>-eq.m<sup>-2</sup>) amounted to 9.5% and 12.9% of the CO<sub>2</sub> emissions at the

wetter plot 1 and only 3.6% during 2011–2012. At the drier plot 2, the CH<sub>4</sub> emissions never amounted to more than 2.3% of the CO<sub>2</sub> emissions.

This study suggests that forest management strategies aiming at enhancing the carbon sink strength in forests also need to consider the impact of forest management on the fluxes of CH<sub>4</sub> and N<sub>2</sub>O since these can contribute with approx. 10% each of the measured CO<sub>2</sub> emissions during individual years. From the 20-year perspective, the importance of CH<sub>4</sub> fluxes (GWP<sub>20</sub> = 84) increases three-fold, which has to be taken into account for any management strategy aiming at maximizing the mitigation potential of forests in the near future.

In addition, the impact of a future, possibly more variable climate with increased frequency and intensity of precipitation events, more extreme temperatures and droughts on GHG budgets should also be considered when implementing forest management policies and practices aiming at enhancing the mitigation potential of forests.

## 5. Conclusions

We measured the fluxes of CO<sub>2</sub>, CH<sub>4</sub>, and N<sub>2</sub>O using a flux-gradient technique at a clear-cut hemiboreal forest stand during three consecutive years, starting one year after the clear-cutting. The method proved to be a reasonable compromise between cost (of instruments, maintenance, running costs, etc.), data coverage and accuracy, and was well suited for inter-plot comparisons even in a heavily disturbed ecosystem. However, future studies should address the large spatial variability in soil properties, soil temperature, soil moisture, etc., as well as soil biogeochemistry to allow more rigorous and robust gap-filling strategies for CH<sub>4</sub> and N<sub>2</sub>O fluxes and to make it possible to obtain a better insight into which processes control the GHG fluxes at clear-cut forest sites. Ideally, future studies should also include measurements to disentangle the relative importance of production and consumption of GHGs, and their drivers, in soils at clear-cut forest stands in order to facilitate modeling and upscaling efforts.

We observed significant emissions of GHGs both at a wet and a dry plot. The relative contribution of CO<sub>2</sub>, CH<sub>4</sub> and N<sub>2</sub>O to the GHG budget differed depending on the degree of wetness, which affected GHG fluxes both directly and indirectly. The faster establishment of vegetation on the wet plot resulted in lower net emissions of CO<sub>2</sub> but this was partially offset by significantly higher CH<sub>4</sub> emissions than at the dry plot 2. It seems likely that waterlogging after clear-cutting caused both plots to switch from a net sink to a net source of CH<sub>4</sub>. We observed significant N<sub>2</sub>O emissions at both plots. The short periods with a low net N<sub>2</sub>O uptake at the wet plot 1 were likely a consequence of an increased reduction of N<sub>2</sub>O to N<sub>2</sub> by denitrifying bacteria during periods when the groundwater table was at, or close to, the surface.

Any policy aiming at enhancing the mitigation potential of forests should consider the combined effect on the climate system of GHG fluxes following forest management operations and also consider what impact a future, more variable climate might have on GHG budgets of forests.

**Author Contributions:** Conceptualization, P.V. and A.L.; methodology, P.V., M.M., L.K. and A.L.; formal analysis, investigation and data curation, P.V., N.K., Z.C., A.H., J.H.; writing—original draft preparation, P.V., N.K., Z.C., A.H.; writing—review and editing, P.V., A.H., Z.C., N.K. and A.L.; visualization, P.V., N.K., Z.C. and A.H.; funding acquisition, N.K. and A.L. All authors have read and agreed to the published version of the manuscript.

**Funding:** Support for this work was provided by The Swedish Energy Agency (grant 31746-1), the Swedish Research Council (grant 621-2007-4704) and by the Linnaeus Centre LUCCI (<http://www.lucci.lu.se/>) funded by the Swedish Research Council. Air-borne LiDAR and digital photography for the Norunda site was acquired with support from the British Natural Environment Research Council (NERC/ARSF/FSF grant EU10-01 and NERC/GEF grant 933). ICOS Sweden is co-funded by the Swedish Research Council (grant 2015-06020).

**Acknowledgments:** We are thankful for all field assistance by Anders Båth and Irene Lehner at the ICOS Sweden station Norunda ([http://www.icos-sweden.se/station\\_norunda.html](http://www.icos-sweden.se/station_norunda.html)) and by Per Weslien from the Department of Earth Sciences at University of Gothenburg. We are grateful to Damien Sulla-Menashe and Eli from Department of Earth and Environment, Boston University for providing the Landsat data. We thank Laura Chasmer, University of Lethbridge, for her help with processing the LiDAR data.

**Conflicts of Interest:** The authors declare no conflict of interest. The funders had no role in the design of the study; in the collection, analyses, or interpretation of data; in the writing of the manuscript, or in the decision to publish the results.

## References

- Pan, Y.; Birdsey, R.A.; Fang, J.; Houghton, R.; Kauppi, P.E.; Kurz, W.A.; Phillips, O.L.; Shvidenko, A.; Lewis, S.L.; Canadell, J.G.; et al. A Large and Persistent Carbon Sink in the World's Forests. *Science* **2011**, *333*, 988–993. [[CrossRef](#)]
- Le Quéré, C.; Raupach, M.R.; Canadell, J.G.; Marland, G.; Bopp, L.; Ciais, P.; Conway, T.J.; Dpney, S.C.; Feely, R.A.; Foster, P.; et al. Trends in the sources and sinks of carbon dioxide. *Nat. Geosci.* **2009**, *2*, 831–836. [[CrossRef](#)]
- Friedlingstein, P.; Jones, M.; O'sullivan, M.; Andrew, R.; Hauck, J.; Peters, G.; Peters, W.; Pongratz, J.; Stich, S.; Le Quéré, C.; et al. Global Carbon Budget 2019. *Earth Syst. Sci. Data* **2019**, *11*, 1783–1838. [[CrossRef](#)]
- Canadell, J.G.; Raupach, R.M. Managing Forests for Climate Change Mitigation. *Science* **2008**, *320*, 1456–1457. [[CrossRef](#)] [[PubMed](#)]
- UNFCCC. *Report of the Conference of the Parties on Its Twenty-First Session, Held in Paris from 30 November to 13 December 2015, Part Two: Action Taken by the Conference of the Parties at Its Twenty-First Session. FCCC/CP/2015/10/Add.1*; United Nations Framework Convention on Climate Change: Paris, France, 2016.
- Luyssaert, S.; Marie, G.; Valade, A.; Chen, Y.Y.; Djomo, S.N.; Ryder, J.; Otto, J.; Naodts, K.; Lansø, A.S.; Ghattas, J.; et al. Trade-offs in using European forests to meet climate objectives. *Nature* **2018**, *562*, 259–262. [[CrossRef](#)] [[PubMed](#)]
- Naudts, K.; Chen, Y.; McGrath, M.J.; Ryder, J.; Valade, A.; Otto, J.; Luyssaert, S. Europe's forest management did not mitigate climate warming. *Science* **2016**, *351*, 597–600. [[CrossRef](#)]
- Swedish Forest Agency. *Statistical Database on Forestry*; Official Statistics of Sweden: Stockholm, Sweden, 2017.
- Smith, K.A.; Dobbie, K.E.; Ball, B.C.; Bakken, L.R.; Sitaula, B.K.; Hansen, S.; Brumme, R.; Borken, W.; Christensen, S.; Priemé, A.; et al. Oxidation of atmospheric methane in Northern European soils, comparison with other ecosystems, and uncertainties in the global terrestrial sink. *Glob. Chang. Biol.* **2000**, *6*, 791–803. [[CrossRef](#)]
- Harriss, R.C.; Sebach, D.I.; Day, P.F. Methane flux in the Great Dismal Swamp. *Nature* **1982**, *297*, 673–674. [[CrossRef](#)]
- Ehhalt, D.H. The atmospheric cycle of methane. *Tellus* **1974**, *26*, 58–70. [[CrossRef](#)]
- von Fischer, C.J.; Hedin, L.O. Separating methane production and consumption with a field-based isotope pool dilution technique. *Glob. Biogeochem. Cycles* **2002**, *16*, 8–1–8–13. [[CrossRef](#)]
- Castro, M.S.; Gholz, H.L.; Clark, K.L.; Steudler, P.A. Effects of forest harvesting on soil methane fluxes in Florida slash pine plantations. *Can. J. For. Res.* **2000**, *30*, 1534–1542. [[CrossRef](#)]
- Sundqvist, E.; Vestin, P.; Crill, P.; Persson, T.; Lindroth, A. Short-Term effects of thinning, clear-cutting and stump harvesting on methane exchange in a boreal forest. *Biogeosciences* **2014**, *11*, 6095–6105. [[CrossRef](#)]
- Sundqvist, E.; Vestin, P.; Crill, P.; Persson, T.; Lindroth, A. Greenhouse gas and energy fluxes in a boreal peatland forest after clear-cutting. *Biogeosciences* **2019**, *16*, 3703–3723.
- Zerva, A.; Mencuccini, M. Short-Term effects of clearfelling on soil CO<sub>2</sub>, CH<sub>4</sub>, and N<sub>2</sub>O fluxes in a Sitka spruce plantation. *Soil Biol. Biochem.* **2005**, *37*, 2025–2036. [[CrossRef](#)]
- Kirschke, S.; Bousquet, P.; Ciais, P.; Saunois, M.; Canadell, J.G.; Dlugokencky, E.J.; Bergamaschi, P.; Bergmann, D.; Blake, D.R.; Bruhwiler, L.; et al. Three decades of global methane sources and sinks. *Nat. Geosci.* **2013**, *6*, 813–823. [[CrossRef](#)]
- Dutaur, L.; Verchot, L.V. A global inventory of the soil CH<sub>4</sub> sink. *Glob. Biogeochem. Cycles* **2007**, *21*, 1–9. [[CrossRef](#)]
- Yu, L.; Huang, Y.; Zhang, W.; Li, T.; Sun, W. Methane uptake in global forest and grassland soils from 1981 to 2010. *Sci. Total Environ.* **2017**, *607–608*, 1163–1172. [[CrossRef](#)]
- Ni, X.; Groffman, P.M. Declines in methane uptake in forest soils. *Proc. Natl. Acad. Sci. USA* **2018**, *115*, 8587–8590. [[CrossRef](#)]

21. Butterbach-Bahl, K.; Baggs, E.M.; Dannenmann, M.; Kiese, R.; Zechmeister-Boltenstern, S. Nitrous oxide emissions from soils: How well do we understand the processes and their controls? *Philos. Trans. R. Soc. B Biol. Sci.* **2013**, *368*, 20130122. [[CrossRef](#)]
22. Bremner, J.M. Sources of nitrous oxide in soils. *Nutr. Cycl. Agroecosyst.* **1997**, *49*, 7–16. [[CrossRef](#)]
23. Schmidt, I.; van Spanning, R.J.M.; Jetten, M.S.M. Denitrification and ammonia oxidation by *Nitrosomonas europaea* wild-type, and NirK- and NorB-deficient mutants. *Microbiology* **2004**, *150*, 4107–4114. [[CrossRef](#)] [[PubMed](#)]
24. Pihlatie, M.; Rinne, J.; Ambus, P.; Pilegaard, K.; Dorsey, J.R.; Rannik, Ü.; Markkanen, T.; Launiainen, S.; Vesala, T. Nitrous oxide emissions from a beech forest floor measured by eddy covariance and soil enclosure techniques. *Biogeosciences* **2005**, *2*, 377–387. [[CrossRef](#)]
25. Mammarella, I.; Werle, P.; Pihlatie, M.; Eugster, W.; Haapanala, S.; Kiese, R.; Markkanen, T.; Rannik, Ü.; Vesala, T. A case study of eddy covariance flux of N<sub>2</sub>O measured within forest ecosystems: Quality control and flux error analysis. *Biogeosciences* **2010**, *7*, 427–440. [[CrossRef](#)]
26. Eugster, W.; Zeyer, K.; Zeeman, M.J.; Michna, P.; Zingg, A.; Buchmann, N.; Emmenegger, L. Methodical study of nitrous oxide eddy covariance measurements using quantum cascade laser spectrometry over a Swiss forest. *Biogeosciences* **2007**, *4*, 927–939. [[CrossRef](#)]
27. Schiller, L.C.; Hastie, D.R. Nitrous oxide and methane fluxes from perturbed and unperturbed boreal forest sites in northern Ontario. *J. Geophys. Res.-Atmos.* **1996**, *101*, 22767–22774. [[CrossRef](#)]
28. Strömgren, M.; Hedwall, P.O.; Olsson, B.A. Effects of stump harvest and site preparation on N<sub>2</sub>O and CH<sub>4</sub> emissions from boreal forest soils after clear-cutting. *For. Ecol. Manag.* **2016**, *371*, 15–22. [[CrossRef](#)]
29. Chapuis-Lardy, L.Y.D.I.E.; Wrage, N.; Metay, A.; CHOTTE, J.L.; Bernoux, M. Soils, a sink for N<sub>2</sub>O? A review. *Glob. Chang. Biol.* **2007**, *13*, 1–17. [[CrossRef](#)]
30. Firestone, M.; Davidson, E. *Microbiological Basis of NO and N<sub>2</sub>O Production and Consumption in Soil, in Exchange of Trace Gases between Terrestrial Ecosystems and the Atmosphere: Report of the Dahlem Workshop on Exchange of Trace Gases between Terrestrial Ecosystems and The Atmosphere*; Andreae, M.O., Schimel, D.S., Eds.; Wiley: New York, NY, USA, 1989; pp. 7–21.
31. Merbold, L.; Eugster, W.; Stieger, J.; Zahniser, M.; Nelson, D.; Buchmann, N. Greenhouse gas budget (CO<sub>2</sub>, CH<sub>4</sub> and N<sub>2</sub>O) of intensively managed grassland following restoration. *Glob. Chang. Biol.* **2014**, *20*, 1913–1928. [[CrossRef](#)]
32. Peichl, M.; Arain, A.M.; Moore, T.R.; Brodeur, J.J.; Khomik, M.; Ullah, S.; Restrepo-Coupe, N.; McLaren, J.; Pejam, M.R. Carbon and greenhouse gas balances in an age sequence of temperate pine plantations. *Biogeosciences* **2014**, *11*, 5399–5410. [[CrossRef](#)]
33. Amiro, B.D.; Barr, A.G.; Barr, J.G.; Black, T.A.; Bracho, R.; Brown, M.; Chen, J.; Clark, K.L.; Davis, K.J.; Desai, A.R.; et al. Ecosystem carbon dioxide fluxes after disturbance in forests of North America. *J. Geophys. Res.* **2010**, *115*, 1–13. [[CrossRef](#)]
34. Coursolle, C.; Margolis, H.A.; Giasson, M.A.; Bernier, P.Y.; Amiro, B.D.; Arain, M.A.; Braa, A.G.; Black, T.A.; Goulden, M.L.; McCaughey, J.H.; et al. Influence of stand age on the magnitude and seasonality of carbon fluxes in Canadian forests. *Agric. For. Meteorol.* **2012**, *165*, 136–148. [[CrossRef](#)]
35. Lindroth, A.; Lagergren, F.; Grelle, A.; Klemetsson, L.; Langvall, O.L.A.; Weslien, P.; Tuulik, J. Storms can cause Europe-wide reduction in forest carbon sink. *Glob. Chang. Biol.* **2009**, *15*, 346–355. [[CrossRef](#)]
36. Lindroth, A.; Grelle, A.; Lankreijer, H.; Båth, A.; Lagergren, F.; Sedletski, A. Partner 4: LUPG. Age-related dynamics of carbon exchange in European forests. In *CARBO-AGE Final Report and Technological Implementation Plan*; Grace, J., Ed.; University of Edinburgh: Edinburgh, UK, 2003; pp. 57–70.
37. Kowalski, A.S.; Loustau, D.; Berbigier, P.; Manca, G.; Tedeschi, V.; Borghetti, M.; Valentini, R.; Kolari, P.; Berninger, F.; Rannik, Ü.; et al. Paired comparisons of carbon exchange between undisturbed and regenerating stands in four managed forests in Europe. *Glob. Chang. Biol.* **2004**, *10*, 1707–1723. [[CrossRef](#)]
38. Kowalski, S.; Sartore, M.; Burlett, R.; Berbigier, P.; Loustau, D. The annual carbon budget of a French pine forest (*Pinus pinaster*) following harvest. *Glob. Chang. Biol.* **2003**, *9*, 1051–1065. [[CrossRef](#)]
39. Kolari, P.; Pumpanen, J.; Rannik, Ü.; Ilvesniemi, H.; Hari, P.; Berninger, F. Carbon balance of different aged Scots pine forests in Southern Finland. *Glob. Chang. Biol.* **2004**, *10*, 1106–1119. [[CrossRef](#)]
40. Humphreys, E.R.; Andrew Black, T.; Morgenstern, K.A.I.; Li, Z.; Nesic, Z. Net ecosystem production of a Douglas-fir stand for 3 years following clearcut harvesting. *Glob. Chang. Biol.* **2005**, *11*, 450–464. [[CrossRef](#)]

41. Misson, L.; Tang, J.; Xu, M.; McKay, M.; Goldstein, A. Influences of recovery from clear-cut, climate variability, and thinning on the carbon balance of a young ponderosa pine plantation. *Agric. For. Meteorol.* **2005**, *130*, 207–222. [[CrossRef](#)]
42. Bergeron, O.; Margolis, H.A.; Coursolle, C.; Giasson, M.A. How does forest harvest influence carbon dioxide fluxes of black spruce ecosystems in eastern North America? *Agric. For. Meteorol.* **2008**, *148*, 537–548. [[CrossRef](#)]
43. Coursolle, C.; Giasson, M.A.; Margolis, H.A.; Bernier, P.Y. Moving towards carbon neutrality: CO<sub>2</sub> exchange of a black spruce forest ecosystem during the first 10 years of recovery after harvest. *Can. J. For. Res.* **2012**, *42*, 1908–1918. [[CrossRef](#)]
44. Williams, C.A.; Vanderhoof, M.K.; Khomik, M.; Ghimire, B. Post-Clearcut dynamics of carbon, water and energy exchanges in a midlatitude temperate, deciduous broadleaf forest environment. *Glob. Chang. Biol.* **2014**, *20*, 992–1007. [[CrossRef](#)]
45. Paul-Limoges, E.; Black, T.A.; Christen, A.; Nesic, Z.; Jassal, R.S. Effect of clearcut harvesting on the carbon balance of a Douglas-Fir forest. *Agric. For. Meteorol.* **2015**, *203*, 30–42. [[CrossRef](#)]
46. Mamkin, V.; Kurbatova, J.; Avilov, V.; Ivanov, D.; Kuricheva, O.; Varlagin, A.; Yaseneva, I.; Olchev, A. Energy and CO<sub>2</sub> exchange in an undisturbed spruce forest and clear-cut in the Southern Taiga. *Agric. For. Meteorol.* **2019**, *265*, 252–268. [[CrossRef](#)]
47. Mamkin, V.V.; Avilov, V.K.; Ivanov, D.G.; Olchev, A.V.; Kurbatova, J.A. CO<sub>2</sub> Fluxes at the Clear-Cut in the Southern Taiga of European Russia. *Contemp. Probl. Ecol.* **2019**, *12*, 491–501. [[CrossRef](#)]
48. Pattey, E.; Strachan, I.B.; Desjardins, R.L.; Edwards, G.C.; Dow, D.; MacPherson, J.I. Application of a tunable diode laser to the measurement of CH<sub>4</sub> and N<sub>2</sub>O fluxes from field to landscape scale using several micrometeorological techniques. *Agric. For. Meteorol.* **2006**, *136*, 222–236. [[CrossRef](#)]
49. Smeets, C.J.P.P.; Holzinger, R.; Vigano, I.; Goldstein, A.H.; Röckmann, T. Eddy covariance methane measurements at a Ponderosa pine plantation in California. *Atmos. Chem. Phys.* **2009**, *9*, 8365–8375. [[CrossRef](#)]
50. Sakabe, A.; Hamotani, K.; Kosugi, Y.; Ueyama, M.; Takahashi, K.; Kanazawa, A.; Itoh, M. Measurement of methane flux over an evergreen coniferous forest canopy using a relaxed eddy accumulation system with tuneable diode laser spectroscopy detection. *Theor. Appl. Climatol.* **2012**, *109*, 39–49. [[CrossRef](#)]
51. Bowling, D.R.; Miller, J.B.; Rhodes, M.E.; Burns, S.P.; Monson, R.K.; Baer, D. Soil, plant, and transport influences on methane in a subalpine forest under high ultraviolet irradiance. *Biogeosciences* **2009**, *6*, 1311–1324. [[CrossRef](#)]
52. Querino, C.A.S.; Smeets, C.J.P.P.; Vigano, I.; Holzinger, R.; Moura, V.; Gatti, L.V.; Martinewski, A.; de Araújo, A.C.; Röckmann, T. Methane flux, vertical gradient and mixing ratio measurements in a tropical forest. *Atmos. Chem. Phys.* **2011**, *11*, 7943–7953. [[CrossRef](#)]
53. Simpson, I.J.; Edwards, G.C.; Thurtell, G.W.; Den Hartog, G.; Neumann, H.H.; Staebler, R.M. Micrometeorological measurements of methane and nitrous oxide exchange above a boreal aspen forest. *J. Geophys. Res. Atmos.* **1997**, *102*, 29331–29341. [[CrossRef](#)]
54. Zona, D.; Janssens, I.A.; Aubinet, M.; Gioli, B.; Vicca, S.; Fichot, R.; Ceulemans, R. Fluxes of the greenhouse gases (CO<sub>2</sub>, CH<sub>4</sub> and N<sub>2</sub>O) above a short-rotation poplar plantation after conversion from agricultural land. *Agric. For. Meteorol.* **2013**, *169*, 100–110. [[CrossRef](#)]
55. Gao, S.; Chen, J.; Tang, Y.; Xie, J.; Zhang, R.; Tang, J.; Zhang, X. Ecosystem carbon (CO<sub>2</sub> and CH<sub>4</sub>) fluxes of a *Populus deltoides* plantation in subtropical China during and post clear-cutting. *For. Ecol. Manag.* **2015**, *357*, 206–219. [[CrossRef](#)]
56. Mishurov, M.; Kiely, G. Nitrous oxide flux dynamics of grassland undergoing afforestation. *Agric. Ecosyst. Environ.* **2010**, *139*, 59–65. [[CrossRef](#)]
57. Dore, S.; Fry, D.L.; Stephens, S.L. Spatial heterogeneity of soil CO<sub>2</sub> efflux after harvest and prescribed fire in a California mixed conifer forest. *For. Ecol. Manag.* **2014**, *319*, 150–160. [[CrossRef](#)]
58. Mjöfors, K.; Strömberg, M.; Nohrstedt, H.Ö.; Gårdenäs, A.I. Impact of site-preparation on soil-surface CO<sub>2</sub> fluxes and litter decomposition in a clear-cut in Sweden. *Silva Fenn.* **2015**, *49*, 1403. [[CrossRef](#)]
59. Strömberg, M.; Mjöfors, K.; Olsson, B.A. Soil-surface CO<sub>2</sub> flux during the first 2 years after stump harvesting and site preparation in 14 Swedish forests. *Scand. J. For. Res.* **2017**, *32*, 213–221. [[CrossRef](#)]

60. Gough, C.M.; Seiler, J.R.; Wiseman, P.E.; Maier, C.A. Soil CO<sub>2</sub> efflux in loblolly pine (*Pinus taeda* L.) plantations on the Virginia Piedmont and South Carolina Coastal Plain over a rotation-length chronosequence. *Biogeochemistry* **2005**, *73*, 127–147. [[CrossRef](#)]
61. Saari, A.; Smolander, A.; Martikainen, P.J. Methane consumption in a frequently nitrogen-fertilized and limed spruce forest soil after clear-cutting. *Soil Use Manag.* **2004**, *20*, 65–73. [[CrossRef](#)]
62. Wu, X.; Brüggemann, N.; Gasche, R.; Papen, H.; Willibald, G.; Butterbach-Bahl, K. Long-Term effects of clear-cutting and selective cutting on soil methane fluxes in a temperate spruce forest in southern Germany. *Environ. Pollut.* **2011**, *159*, 2467–2475. [[CrossRef](#)]
63. McVicar, K.; Kellman, L. Growing season nitrous oxide fluxes across a 125+year harvested red spruce forest chronosequence. *Biogeochemistry* **2014**, *120*, 225–238. [[CrossRef](#)]
64. Saari, P.; Saarnio, S.; Saari, V.; Heinonen, J.; Alm, J. Initial effects of forestry operations on N<sub>2</sub>O and vegetation dynamics in a boreal peatland buffer. *Plant Soil* **2010**, *330*, 149–162. [[CrossRef](#)]
65. Huttunen, J.T.; Nykänen, H.; Martikainen, P.J.; Nieminen, M. Fluxes of nitrous oxide and methane from drained peatlands following forest clear-felling in southern Finland. *Plant Soil* **2003**, *255*, 457–462. [[CrossRef](#)]
66. Saari, P.; Saarnio, S.; Kukkonen, J.V.; Akkanen, J.; Heinonen, J.; Saari, V.; Alm, J. DOC and N<sub>2</sub>O dynamics in upland and peatland forest soils after clear-cutting and soil preparation. *Biogeochemistry* **2009**, *94*, 217–231. [[CrossRef](#)]
67. Lavoie, M.; Kellman, L.; Risk, D. The effects of clear-cutting on soil CO<sub>2</sub>, CH<sub>4</sub>, and N<sub>2</sub>O flux, storage and concentration in two Atlantic temperate forests in Nova Scotia, Canada. *For. Ecol. Manag.* **2013**, *304*, 355–369. [[CrossRef](#)]
68. Kulmala, L.; Aaltonen, H.; Berninger, F.; Kieloaho, A.J.; Levula, J.; Bäck, J.; Hari, P.; Kolari, P.; Korhonen, J.F.J.; Kulmala, M.; et al. Changes in biogeochemistry and carbon fluxes in a boreal forest after the clear-cutting and partial burning of slash. *Agric. For. Meteorol.* **2014**, *188*, 33–44. [[CrossRef](#)]
69. Oren, R.A.M.; Hsieh, C.I.; Stoy, P.; Albertson, J.; McCarthy, H.R.; Harrell, P.; Katul, G.G. Estimating the uncertainty in annual net ecosystem carbon exchange: Spatial variation in turbulent fluxes and sampling errors in eddy-covariance measurements. *Glob. Chang. Biol.* **2006**, *12*, 883–896. [[CrossRef](#)]
70. Hill, T.; Chocholek, M.; Clement, R. The case for increasing the statistical power of eddy covariance ecosystem studies: Why, where and how? *Glob. Chang. Biol.* **2017**, *23*, 2154–2165. [[CrossRef](#)]
71. Denmead, O.T. Approaches to measuring fluxes of methane and nitrous oxide between landscapes and the atmosphere. *Plant Soil* **2008**, *309*, 5–24. [[CrossRef](#)]
72. Lundin, L.C.; Halldin, S.; Lindroth, A.; Cienciala, E.; Grelle, A.; Hjelm, P.; Kellner, E.; Lendberg, N.; Mölder, M.; Morén, A.-S. Continuous long-term measurements of soil-plant-atmosphere variables at a forest site. *Agric. For. Meteorol.* **1999**, *98–99*, 53–73. [[CrossRef](#)]
73. Oliver, M.A.; Webster, R. Kriging: A method of interpolation for geographical information systems. *Int. J. Geogr. Inf. Syst.* **1990**, *4*, 313–332. [[CrossRef](#)]
74. Schmid, H.P.; Grimmond, C.S.B.; Cropley, F.; Offerle, B.; Su, H.B. Measurements of CO<sub>2</sub> and energy fluxes over a mixed hardwood forest in the mid-western United States. *Agric. For. Meteorol.* **2000**, *103*, 357–374. [[CrossRef](#)]
75. Vickers, D.; Mahrt, L. Quality Control and Flux Sampling Problems for Tower and Aircraft Data. *J. Atmos. Ocean. Technol.* **1997**, *14*, 512–526. [[CrossRef](#)]
76. Nakai, T.; Shimoyama, K. Ultrasonic anemometer angle of attack errors under turbulent conditions. *Agric. For. Meteorol.* **2012**, *162–163*, 14–26. [[CrossRef](#)]
77. Moncrieff, J.; Clement, R.; Finnigan, J.; Meyers, T. *Averaging, Detrending and Filtering of Eddy Covariance Time Series*, in *Handbook of Micrometeorology: A Guide for Surface Flux Measurements*; Lee, X., Massman, W.J., Law, B.E., Eds.; Springer: Dordrecht, The Netherlands, 2004; pp. 7–31.
78. Moncrieff, J.B.; Massheder, J.M.; De Bruin, H.; Elbers, J.; Friborg, T.; Heusinkveld, B.; Kabat, P.; Scott, S.; Soegaard, H.; Verhoef, A. A system to measure surface fluxes of momentum, sensible heat, water vapour and carbon dioxide. *J. Hydrol.* **1997**, *188*, 589–611. [[CrossRef](#)]
79. Desjardins, R.L.; MacPherson, J.I.; Schuepp, P.H.; Karanja, F. An evaluation of aircraft flux measurements of CO<sub>2</sub>, water vapor and sensible heat. *Bound. Layer Meteorol.* **1989**, *47*, 55–69. [[CrossRef](#)]
80. Oncley, S.P.; Friehe, C.A.; Larue, J.C.; Businger, J.A.; Itsweire, E.C.; Chang, S.S. Surface-Layer Fluxes, Profiles, and Turbulence Measurements over Uniform Terrain under Near-Neutral Conditions. *J. Atmos. Sci.* **1996**, *53*, 1029–1044. [[CrossRef](#)]

81. Högström, U. Non-Dimensional wind and temperature profiles in the atmospheric surface layer: A re-evaluation. *Bound. Layer Meteorol.* **1988**, *42*, 55–78.
82. Foken, T. *Micrometeorology*; Springer: Berlin/Heidelberg, Germany, 2017; p. 362.
83. Wieringa, J. Representative roughness parameters for homogeneous terrain. *Bound. Layer Meteorol.* **1993**, *63*, 323–363. [[CrossRef](#)]
84. Kljun, N.; Calanca, P.; Rotach, M.W.; Schmid, H.P. A simple two-dimensional parameterisation for Flux Footprint Prediction (FFP). *Geosci. Model Dev.* **2015**, *8*, 3695–3713. [[CrossRef](#)]
85. Horst, T.W. The Footprint for Estimation of Atmosphere-Surface Exchange Fluxes by Profile Techniques. *Bound. Layer Meteorol.* **1999**, *90*, 171–188. [[CrossRef](#)]
86. Mauder, M.; Foken, T. *Documentation and Instruction Manual of the Eddy Covariance Software Package TK2*; Universität Bayreuth: Bayreuth, Germany, 2004; p. 44.
87. Wutzler, T.; Lucas-Moffat, A.; Migliavacca, M.; Knauer, J.; Sickel, K.; Šigut, L.; Reichstein, M. Basic and extensible post-processing of eddy covariance flux data with REddyProc. *Biogeosciences* **2018**, *15*, 5015–5030. [[CrossRef](#)]
88. Reichstein, M.; Falge, E.; Baldocchi, D.; Papale, D.; Aubinet, M.; Berbigier, P.; Bernhofer, C.; Buchmann, N.; Gilmanov, T.; Granier, A.; et al. On the separation of net ecosystem exchange into assimilation and ecosystem respiration: Review and improved algorithm. *Glob. Chang. Biol.* **2005**, *11*, 1424–1439. [[CrossRef](#)]
89. Lloyd, J.; Taylor, J.A. On the Temperature Dependence of Soil Respiration. *Funct. Ecol.* **1994**, *8*, 315–323. [[CrossRef](#)]
90. Scanlon, M.T.; Kiely, G. Ecosystem-Scale measurements of nitrous oxide fluxes for an intensely grazed, fertilized grassland. *Geophys. Res. Lett.* **2003**, *30*, 1–4. [[CrossRef](#)]
91. Myhre, G.; Shindell, D.; Bréon, F.-M.; Collins, W.; Fuglestvedt, J.; Huang, J.; Koch, D.; Lamarque, J.-F.; Lee, D.; Mendoza, B.; et al. *Climate Change 2013: The Physical Science Basis. Contribution of Working Group I to the Fifth Assessment Report of the Intergovernmental Panel on Climate Change*; Stocker, T.F., Qin, D., Plattner, G.-K.I., Tignor, M., Allen, S.K., Boschung, J., Nauels, A., Xia, Y., Bex, V., Midgley, P.M., Eds.; Cambridge University Press: Cambridge, UK; New York, NY, USA, 2013.
92. Zhu, Z.; Woodcock, C.E. Object-Based cloud and cloud shadow detection in Landsat imagery. *Remote. Sens. Environ.* **2012**, *118*, 83–94. [[CrossRef](#)]
93. Zhu, Z.; Wang, S.; Woodcock, C.E. Improvement and expansion of the Fmask algorithm: Cloud, cloud shadow, and snow detection for Landsats 4–7, 8, and Sentinel 2 images. *Remote. Sens. Environ.* **2015**, *159*, 269–277. [[CrossRef](#)]
94. Tucker, C.J. Red and photographic infrared linear combinations for monitoring vegetation. *Remote. Sens. Environ.* **1979**, *8*, 127–150. [[CrossRef](#)]
95. Rinne, J.; Riutta, T.; Pihlatie, M.; Aurela, M.; Haapanala, S.; Tuovinen, J.P.; Tuittila, E.-S.; Vesala, T. Annual cycle of methane emission from a boreal fen measured by the eddy covariance technique. *Tellus B* **2007**, *59*, 449–457. [[CrossRef](#)]
96. Tagesson, T.; Mölder, M.; Mastepanov, M.; Sigsgaard, C.; Tamstorf, M.P.; Lund, M.; Falk, J.M.; Lindroth, A.; Christensen, T.R.; Ström, L. Land-Atmosphere exchange of methane from soil thawing to soil freezing in a high-Arctic wet tundra ecosystem. *Glob. Chang. Biol.* **2012**, *18*, 1928–1940. [[CrossRef](#)]
97. Dengel, S.; Zona, D.; Sachs, T.; Aurela, M.; Jammot, M.; Parmentier, F.J.W.; Oechel, W.; Vesala, T. Testing the applicability of neural networks as a gap-filling method using CH<sub>4</sub> flux data from high latitude wetlands. *Biogeosciences* **2013**, *10*, 8185–8200. [[CrossRef](#)]
98. Sundqvist, E.; Persson, A.; Kljun, N.; Vestin, P.; Chasmer, L.; Hopkinson, C.; Lindroth, A. Upscaling of methane exchange in a boreal forest using soil chamber measurements and high-resolution LiDAR elevation data. *Agric. For. Meteorol.* **2015**, *214–215*, 393–401. [[CrossRef](#)]
99. Mishurov, M.; Kiely, G. Gap-Filling techniques for the annual sums of nitrous oxide fluxes. *Agric. For. Meteorol.* **2011**, *151*, 1763–1767. [[CrossRef](#)]
100. Teepe, R.; Brumme, R.; Beese, F.; Ludwig, B. Nitrous Oxide Emission and Methane Consumption Following Compaction of Forest Soils. *Soil Sci. Soc. Am. J.* **2004**, *68*, 605–611. [[CrossRef](#)]
101. Tate, K.R.; Ross, D.J.; Scott, N.A.; Rodda, N.J.; Townsend, J.A.; Arnold, G.C. Post-Harvest patterns of carbon dioxide production, methane uptake and nitrous oxide production in a *Pinus radiata* D. Don plantation. *For. Ecol. Manag.* **2006**, *228*, 40–50. [[CrossRef](#)]

102. Dunfield, P.; Dumont, R.; Moore, T.R. Methane production and consumption in temperate and subarctic peat soils: Response to temperature and pH. *Soil Biol. Biochem.* **1993**, *25*, 321–326. [[CrossRef](#)]
103. Wang, J.M.; Murphy, J.G.; Geddes, J.A.; Winsborough, C.L.; Basiliko, N.; Thomas, S.C. Methane fluxes measured by eddy covariance and static chamber techniques at a temperate forest in central Ontario, Canada. *Biogeosciences* **2013**, *10*, 4371–4382. [[CrossRef](#)]
104. Sundqvist, E.; Mölder, M.; Crill, P.; Kljun, N.; Lindroth, A. Methane exchange in a boreal forest estimated by gradient method. *Tellus B.* **2015**, *67*, 1–16. [[CrossRef](#)]
105. Sundqvist, E.; Crill, P.; Mölder, M.; Vestin, P.; Lindroth, A. Atmospheric methane removal by boreal plants. *Geophys. Res. Lett.* **2012**, *39*, 1–6. [[CrossRef](#)]
106. Ryden, J.C.; Lund, L.J.; Focht, D.D. Direct In-Field Measurement of Nitrous Oxide Flux from Soils. *Soil Sci. Soc. Am. J.* **1978**, *42*, 731–737. [[CrossRef](#)]
107. Denmead, O.T.; Freney, J.R.; Simpson, J.R. Studies of Nitrous Oxide Emission from a Grass Sward. *Soil Sci. Soc. Am. J.* **1979**, *43*, 726–728. [[CrossRef](#)]
108. Blackmer, A.M.; Robbins, S.G.; Bremner, J.M. Diurnal Variability in Rate of Emission of Nitrous Oxide from Soils. *Soil Sci. Soc. Am. J.* **1982**, *46*, 937–942. [[CrossRef](#)]
109. Shurpali, N.J.; Rannik, Ü.; Jokinen, S.; Lind, S.; Biasi, C.; Mammarella, I.; Peltola, O.; Pihlatie, M.; Hyvönen, N.; Rätty, M.; et al. Neglecting diurnal variations leads to uncertainties in terrestrial nitrous oxide emissions. *Sci. Rep.* **2016**, *6*, 25739. [[CrossRef](#)] [[PubMed](#)]
110. Zona, D.; Janssens, I.A.; Gioli, B.; Jungkunst, H.F.; Serrano, M.C.; Ceulemans, R. N<sub>2</sub>O fluxes of a bio-energy poplar plantation during a two years rotation period. *GCB Bioenergy* **2013**, *5*, 536–547. [[CrossRef](#)]
111. Kroon, P.S.; Schrier-Uijl, A.P.; Hensen, A.; Veenendaal, E.M.; Jonker, H.J.J. Annual balances of CH<sub>4</sub> and N<sub>2</sub>O from a managed fen meadow using eddy covariance flux measurements. *Eur. J. Soil Sci.* **2010**, *61*, 773–784. [[CrossRef](#)]
112. Butterbach-Bahl, K.; Rothe, A.; Papen, H. Effect of tree distance on N<sub>2</sub>O and CH<sub>4</sub> -fluxes from soils in temperate forest ecosystems. *Plant Soil* **2002**, *240*, 91–103. [[CrossRef](#)]



© 2020 by the authors. Licensee MDPI, Basel, Switzerland. This article is an open access article distributed under the terms and conditions of the Creative Commons Attribution (CC BY) license (<http://creativecommons.org/licenses/by/4.0/>).